Anatomy of subinertial waves along the Patagonian shelf break in a 1/12° global operational model

Léa Poli, Camila Artana, Christine Provost, Jérôme Sirven, Nathalie Sennéchael, Yannis Cuypers, Jean-Michel Lellouche

Anatomy of subinertial waves along the Patagonian shelf break in a 1/12° global operational model

Léa Poli[1], Camila Artana[2], Christine Provost[1], Jérôme Sirven[1], Nathalie Sennéchael[1], Yannis Cuypers[1], Jean-Michel Lellouche[2]

1) LOCEAN-IPSL, Sorbonne Université (UPMC, Univ. Paris 6)-CNRS-IRD-MNHN, Paris, France
2) MERCATOR OCEAN, Parc Technologique du Canal, Ramonville St. Agne, France

Key points

1- Velocity signals with phase speeds of 140-300 cm/s at the shelf break and 10-30 cm/s in the core of the Malvinas Current were identified.

2- At the shelf break, wind-forced fast waves modulated the inner Malvinas Current jet and possibly contributed to upwelling

3- Slowly propagating waves in the core of the Malvinas Current came from the Malvinas Escarpment or the Drake Passage.

Key words:

topographic waves, shelf break, Malvinas Current, jets, upwelling, global operational model, Current-meter data.

Abstract :

The Patagonian slope hosts a variety of waves. We used a state of the art ocean reanalysis to examine waves at the shelf break and in the core of the Malvinas Current (MC) at periods larger than 10 days. Statistics over 25 years indicated three types of signals: in phase signals at specific locations of the shelf break to the south of 47°S, fast propagating signals all along the shelf break (phase speed from 140 cm/s to 300 cm/s) at periods between 5 and 110 days, and slower signals in the core of the MC (phase speeds from 10 cm/s to 30 cm/s) at 20-day, 60-day and 100-day periods.

The large zonal wind stress variations south of 47°S forced in-phase along-slope velocity variations and triggered fast propagating waves at distinct sites corresponding to abrupt changes in the shelf break orientation. The shelf break waves modulated the intensity of the inshore jet, which varied from 0 to 30 cm/s at 100 m depth, and had spatial and temporal structures and scales consistent with those of observed upwelling events. Slow propagating waves in the core of the MC had along-slope wavelengths between 450 and 1200 km and were not forced by the local winds. They were tracked back to the Drake Passage and the Malvinas Escarpment.

Plain language summary:

The sinuous Patagonian slope hosts a variety of waves that are yet poorly documented. We examined the waves in a state of the art ocean model assimilating observations. Strong westerly winds forced fast waves at the shelf break. These waves modulated the intensity of the coastal jet of the Malvinas Current and the shelf break upwelling. Slow waves propagating from the Malvinas Escarpment and the Drake Passage modified the velocities of the Malvinas Current main jet.

1. Introduction

The Malvinas Current (MC), a major western boundary current of the South Atlantic Ocean, is an offshoot of the Antarctic Circumpolar Current (Figure 1a) that flows northward following the Subantarctic Front (SAF) along the eastern continental slope of South America. The MC, which borders one of the widest continental shelf of the world, is strongly controlled by bottom topography. Between 52°S and 49°S the bottom slope is west-east orientated and gentle (2000 m over 300 km) and the MC is rather wide (300 km) with mean northward surface velocities of 30 cm/s (Figures 1a and 1b). At 48°S isobaths are east-west orientated and the MC mean surface velocities are zonal with a mean value of 40 cm/s. The largest mean surface velocities in the MC (> 60 cm/s) are observed north of 43°S where the bottom slope is steep (Figures 1a and 1b) and the MC is organized in one narrow jet. South of 43°S, the MC is characterized by a relatively stable two-jet structure alienated with two bottom terraces (Piola et al., 2013). The mean location of the onshore jet corresponds to a northern branch of the SAF (SAF-N), while the main jet follows the main SAF along the 1500 m isobath (Figure 1b; Artana et al., 2018a). At 38°S the MC encounters the Brazil Current forming the Brazil-Malvinas Confluence. The surface eddy kinetic energy (EKE) at this region is among the greatest in the world ocean with values exceeding 2000 cm^2/s^2 (Figure 1c). In contrast, the EKE in the MC is rather small (200 cm^2/s^2) since the Malvinas Plateau filters a large part of the mesoscale activity from Drake Passage (Artana et al., 2016).

In situ observations have pointed at the possible existence of trapped waves (TW) propagating northward along the Patagonian slope. Velocity spectra obtained from current meters moorings deployed at 41°S across the slope near the Brazil Malvinas Confluence showed large energy peaks between 5 and 110 days (Vivier and Provost

1999; Vivier et al., 2001). Despite these observations there is still no characterization of TW along the Patagonian slope. As the TW propagates rapidly they are not entirely resolved in satellite altimetry-derived maps of sea level anomalies (Ballarotta et al., 2019).

The MC carries cold, nutrient-rich Subantarctic waters that play a key role in the development of the biological activity in this region: massive phytoplankton blooms are observed over the Patagonian shelf (Romero et al., 2006; Valla and Piola, 2015). The inner portion of the Patagonian continental shelf break presents chlorophyll concentrations peaking at 2.5-3.0 mg/m^3 (Figure 1d). TW disturbs the upper thermocline and could enhance the fluxes of nutrients to the shelf break.

High resolution ocean models (1/12°) that assimilate in situ observations and along-track satellite altimetry, such as the Mercator Ocean physical reanalysis at 1/12°, could provide some insights on TW propagating along the Patagonian shelf break. Previous works have assessed the performance of this reanalysis in the MC system (Artana et al., 2018a and Artana et al., 2019). Here we further evaluate the spectral content of the reanalysis sea level anomalies and velocities on the slope compared to observations. As a result of this comparison, we use the reanalysis tri-dimensional fields to examine TWs at the shelf break and in the core of the MC at periods larger than 10 days. The theory from Brink (1982), which idealizes TW as a sum of modes whose spatial structure, phase and group velocities depend upon the cross-shore topography and stratification, provided guidance.

This paper is organized as follows. We first compare possible signatures of trapped waves in observations and the Mercator Ocean reanalysis. In section 3, we explorefast waves detected at the shelf break and interpret them using the idealized model from

Brink and Chapman (1987). Slower velocity variations in the core of the MC above the 1500 m isobath are examined in section 4. Section 5 discusses the results and concludes.

2. Model and data: possible signatures of trapped waves

2.1 Mercator Ocean reanalysis

The high resolution (1/12°) global Mercator Ocean reanalysis (hereafter GLORYS12) has been developed in the framework of the Copernicus Marine Environment Monitoring Service (CMEMS, http://marine.copernicus.eu/) and extends over a period of 25 years (1993-2017). This reanalysis is based on the current real time global forecasting CMEMS system (Lellouche et al., 2018) with a few changes in atmospheric forcing, assimilated data and observation errors. NEMO (Nucleus of European Modeling of the Ocean platform) is the dynamical core of the physical model. The ocean surface is forced by the global ERA-Interim atmospheric reanalysis from the European Center for Medium-Range Weather Forecasts. The model assimilates observations using a reduced order Kalman filter with a 3-D multivariate modal decomposition of the background error and a 7-day assimilation cycle (Lellouche et al., 2018). The model assimilates jointly along track satellite altimetric data from CMEMS (Pujol et al., 2016), AVHRR satellite Sea Surface Temperature from NOAA, Ifremer/CERSAT Sea-Ice Concentration, and in situ temperature and salinity vertical profiles from the latest CORA in situ databases (Cabanes et al., 2013; Szekely et al., 2016). Artana et al. (2018a) evaluated the performance of the reanalysis GLORYS12 over the MC and found a good agreement with observations. Further comparisons on the continental slope between the model and observations are shown below.

2.2 GLORYS12 and satellite altimetry spectral contents along the slope

We used DUACS delayed time altimeter gridded (1/4° regular grid) daily product (Pujol et al., 2016; Taburet et al., 2018) available at http://marine.copernicus.eu/. This product results from an optimal interpolation in space and time, combining measurements from different altimeters and its effective resolution is about 20 days in time and 200 km in space (e.g., Archer et al., 2020).

GLORYS12 produces somewhat larger EKE values on the Patagonian slope than satellite altimetry (Artana et al., 2018a, their figures 1b and 1d). We built a time series of averaged sea level anomaly between the 300 and 1700 m isobaths all along the slope. Their spectra are shown as a function of latitude for the DUACS product (Figure 2a) and GLORYS12 (Figure 2b). The spectra display striking similarities with significant energy peaks at distinct periods between 10 days and 500 days. The annual cycle dominates the spectra. The continuum of energy observed in the spectra to the north of 40°S reflects the outstanding variability at the Brazil-Malvinas confluence. Some periods such as 20, 60-70 and 100 days exhibited energy all along the slope. Those periods could be associated with waves propagating between the 300 and 1700 m isobaths. There was no energy at periods shorter than 5 days in either spectrum, and as expected GLORYS12 displayed more energy than altimetry at periods between 5 and 14days (Figure 2c).

Indeed, satellite gridded data do not capture variations at periods smaller than 14 days.

2.3 GLORYS12 and mooring data on the slope at 41°S

Current meter moorings have been deployed in 1993-1995, 2001-2003 and 2014-2015 across the continental slope at 41°S near the Confluence (Vivier and Provost, 1999;

Spadone and Provost, 2009; Ferrari et al., 2017). As GLORYS12 showed no significant energy at periods shorter than 5 days, the mooring data were 5-day low-pass filtered for comparison. In spite of significant differences from one deployment to the other, means and variance ellipses showed consistent patterns with a mean flow towards the North East and ellipses stretched in the direction of the mean flow above the slope, and weaker mean flow and more round ellipses offshore (Figure 3, 1993-95 in black, 2001-2003 in blue, 2014-2015 in green, GLORYS12 in red). GLORYS12 accurately reproduced the general patterns and the differences between mooring deployments with in particular large variance ellipses during the last deployment due to the Confluence position being exceptionally south from May to September 2015 (Paniagua et al., 2018; Artana et al., 2019). The intensity and direction of the mean flow and the variance ellipses from GLORYS12 were in good agreement with the observations in this highly energetic and complex region (Figure 3).

2.4 Statistics over 25 years: Evidence of different propagation velocities above the 300 and 1500 m isobaths in GLORYS12.

We examined the propagation of along-slope velocity anomalies at 100 m depth following the 300 m isobath of the Patagonian slope (Figure 4). A 110-day high-pass filter was applied to remove the seasonal cycle. The filtered velocities along the 300 m isobath (colored points in Figure 4a) were correlated with those at locations Φ ((60.5°W,53.5°S), Ω (60.5°W,47°S), and Ψ (56.8°W,41°S) (black points in Figure 4a). Lagged correlations are shown as a function of distance from Φ (53.5°S) along the slope (lagged correlations with Φ in Figure 4b, Ω in Figure 4c and Ψ in Figure 4d). For each point along the isobath we selected the lag presenting the maximum correlation and applied a linear fit (dashed lines in Figure 4) to estimate propagation velocities. Correlations with Φ were maximum at lag 0 to the south of km 200 ($r > 0.5$) and

between km 600 and 1050 (0.3< r <0.5, pink dots in Figure 4b), indicating simultaneous signals. In addition, two high-correlation patterns (dashed lines in Figure 4b) suggested northward propagations from Φ and from Ω with a phase speed ranging between 140 and 300 cm/s. The correlations associated with these propagating signals diminished with distance and remained significant until 38°S (km 2100). These features were consistently found in the lagged correlations with point Ω (Figure 4c): maximum correlations at lag 0 nearby Ω and Φ (r > 0.5), and two patterns suggesting the same propagating signals at similar phase speeds (dashed lines in Figure 4c). Lagged correlations with Ψ (Figure 4d) showed a slower (phase speed between 20 and 30 cm/s) and more localized propagation between km 1600 and 2000 (43 and 40°S, with correlations exceeding 0.5) superposed to the faster propagation signals associated with small correlations of 0.25.

Lagged correlations between along-slope velocities above the 1500 m isobath, in the core of the MC, showed more localized features around Φ' (58.6°W, 53.35°S), Ω' (59.2°W, 47°S) and Ψ' (56°W, 41°S) (Figure 5). Correlations at Φ' (r>0.5) suggested no propagation and a period about 40 days (Figure 5b). The correlation pattern with Ω' indicated propagating signals (with r > 0.3) with a phase speed of 20 cm/s with periods of about 50 days extending from km 800 to km 1600 (Figure 5c). Correlation patterns with Ψ' suggested propagating signals with a phase speed of about 25 cm/s and a period of 50 days between km 1600 and 2100 (Figure 5d) . This propagating feature was reminiscent of the one observed at 41°S over the 300 m isobath in Figure 4d.

Statistics over 25 years of GLORYS12 revealed three types of signals: signals merely in phase to the south of 47°S at the shelf break, fast propagating signals with phase speed ranging from 140 to 300 cm/s all along the shelf break, and slower signals in the core of the MC with propagation velocities ranging from 10 to 30 cm/s.

3. Fast signals at the shelf break

3.1 Coherent forced response to wind pulses over the 25 years

The Southwest Atlantic undergoes strong westerlies (Figure 6a) with large wind stress mean values (>0.2 Pa) to the south of 52°S and in the southwestern portion of the deep Argentine Basin. The intensity of the mean wind stress decreases towards the north along the Patagonian slope to 0.05 Pa at 38°S. The zonal wind stress shows a maximum variability (Figure 6b) near Φ.

The zonal wind stress along the slope was highly correlated ($r > 0.8$) with the zonal wind stress at 53.5°S (Φ) up to 47°S (Ω) (not shown). Lagged correlations of the along-slope velocities over the 300 m isobath with the zonal wind stress at Φ (Figure 6c) showed patterns reminiscent of those observed in Figure 4b. Interestingly, correlations at lag 1 day peaked at the distinct locations indicated with pink dots in Figure 6c. These locations showed in-phase along-slope velocity variations (Figure 4b), suggesting a wind-forced quasi-instantaneous response (compare pink dots in figure 4b and 6c). The wind also triggered the fast propagating signals departing from Φ and Ω (previously identified in Figures 4b and 4c). Other wave departures were observed between km 0 and 1000: at km 200, 400, 800, and 1000 (Figure 6c). They corresponded to changes in direction of the bathymetry gradient (indicated with stick plot in Figure 6c).

In contrast, correlations of the zonal wind stress at Φ' and Ω' with the along-slope velocities over the 1500 m isobath (not shown) were not significant suggesting that non-propagating signals and the slow propagations were not forced by the local wind.

Along-slope velocity composites shown in Figures 7b-g were obtained from averaging maps for the dates when the amplitude of the along slope velocity filtered time series

at Φ (Ω and Ψ respectively) exceeded one standard deviation. (Figure 7a). This criterion selected about 1350 (1400) days for the positive (negative) events for each time series.

The composite maps of positive events (Figure 7 b c d) have similar spatial structures with an opposite sign to the negative ones consistent with wave dynamics.

The wind stress anomalies associated with the composites exhibited a well-defined anticyclonic/cyclonic structure centered around the Malvinas Islands with zonal wind anomalies at Φ (Figures 7b and 7e). The wave departure locations identified in Figure 6c corresponded to the locations of the largest along slope velocity anomalies (Figures 7b and 7e). A simultaneous wave departure was seen on the western side of East of Burdwood Bank Passage. As expected the composite maps built from Ω time series are similar to those built from Φ. Composite maps exhibit complex cross-slope structure with changing sign velocities (Figure 7 b-g). The composite built from Ψ showed a weak velocity signal all along the shelf break intensified near Ψ, plus a signal over the 1500 m isobath between 47°S and Ψ (Figures 7d and 7g). These observations were consistent with the superposition of two propagating patterns as seen in Figure 4d, a fast one along the shelf break and a slower one offshore above the 1500 m isobath.

3.2 Idealized ocean response : cross-slope modal structure

We used the linear theory of Brink and Chapman (1987), which provides the modal structures of sub-inertial frequency waves on a sloping bottom under idealized hypotheses (see appendix). In spite of idealized assumptions such as a straight coastline with uniform shelf bathymetry, which is not the case of the Patagonian shelf break, the analysis provided some insight in the modal structure of trapped waves. We

computed cross-slope modal structures of trapped waves along three sections across the Patagonian slope : the first one at 51°S where the slope is gentle and the bottom relatively shallow (2000 m), the second one at 47°S where the upper slope is steeper and the last one at 42°S showing an abrupt bathymetry (Figure 8). The 4 gravest modes and their dispersion curves for the 3 sections are shown in the appendix. Along the cross-slope sections the modes are nearly barotropic, trapped at the shelf break and bottom intensified on the lower slope (see appendix).

Along the three sections, we built velocity composites corresponding to the dates of significant peaks (above the standard deviation) in the along-slope velocities at 100 m above the 300 m isobath (Figure 8). The three velocity composites featured patterns reminiscent of theoretical modes 2, 3 and 4 (see appendix). Mode 2, 3 and 4 dispersion curves provided theoretical phase velocities matching the observed one (about 140 to 300 cm/s) for waves with periods ranging between 5 and 110 days and wavelengths varying from 500 to 2500 km. The theoretical mode is defined within a multiplicative factor (Brink 1989); velocity maxima in the composite and the theoretical mode suggested a scaling factor of 6 10^8. Applying the factor scale to the theoretical mode led to across slope velocities of the order of 1 cm/s, consistent with the across slope composites (not shown) and to vertical velocity estimates of the order of 5-20 m/d.

3.3 Period-wavelength spectrum of along-slope velocities at 100 m above the 300 m isobath.

The period-wavelength spectrum of along slope velocities at 100 m above the 300 m isobath showed energy along patterns consistent with theoretical dispersion relations associated with shelf-break trapped waves of modes 2, 3 and 4 propagating northward (Figure 9). The theoretical dispersion curves computed for several latitudes

with different bottom steepness and mean flows (black and grey lines in Figure 9) show that although the hypothesis of an infinite constant slope is far from being satisfied, the theory provides insight into the dynamics.

We filtered SBTW signals in three period bands (10-40, 30-90 and 80-110 days) and built the corresponding composites (not shown). We obtained similar patterns to those in Figure 7 with wavelengths increasing with periods as expected from theory.

3.4 Impact of the shelf-break waves on the onshore jet

South of 42°S, the MC is organized in two relatively stable jets (Piola et al., 2013).The main jet straddles the 1500 m isobath and corresponds to the main SAF and the largest current core, while the onshore jet associated with the northern branch of the SAF follows the 300 m isobath from west of Burwood Bank at 55°S to 44°S (Figure 1b). We investigated the potential relation between the fast propagating waves and the onshore jet. The positive phase of the wave corresponded to an intensification of the onshore jet along the shelf break from 55°S to 47°S (Figure 10 a). Local along-slope velocity maxima at the shelf break were associated with the regions of wave departure (identified in Figure 6c). The onshore jet split into two branches at 51°S where the 300 and 500 m isobaths diverge. The two branches merged in a single onshore strong jet at 47°S where the two isobaths converge (Figure 10a). At 47°S, the onshore jet reached 40 cm/s near the surface (Figure 10b). In contrast, during the negative phase the onshore jet core velocity diminishes (Figures 10c and 10d).

3.5 Sea surface anomalies accompanying fast shelf-break waves

The GLORYS12 SLA composite maps built from velocity time series at Φ shows a positive/negative signal (> 4 cm) over the continental shelf consistent with the

anticyclonic/cyclonic wind anomaly pattern creating convergence/divergence associated with the positive and negative phase of the wave (Figures 11b and 11e).

Stronger composite SLA patterns were observed on the shelf in the composite for Ω (Figures 11c and 11f).

All along the shelf break composite SLA values were small of the order of 2 cm, however synoptic SLA values at Ω could reach peak values larger than 5 cm lasting less than 10 days (Figure 11a). The SLA composites were consistent with the modes (2-4) predicted by Brink linear theory (Figure A5). In contrast, SLA composites for Ψ (Figures 11d and 11g) showed low values on the continental shelf (amplitude less than 2.5 cm) and a somewhat stronger mesoscale structure of opposite sign (3.5 cm) close to 42°S centered slightly offshore, reminiscent of slow propagating signals observed in Figure 4d.

4. Velocity variations in the core of the Malvinas Current

SLA spectra showed energy distributed in distinct periods ranging from 10 to 110 days all along the slope (Figure 2). To distinguish the different spatial patterns (wavelength) associated with these periods, we band-pass filtered along-slope velocities and SLA in three overlapping period ranges: 10-40, 30-90 and 80-110 days. We focused on the location Ω' at 47°S, a central position along the slope. An example of the velocity and SLA decomposition is shown in Figure 12 for year 2013. The sum of the three filtered time series explained 87% of the velocity variance (73% of the SLA variance) over the 25 years. The 10-40 (30-90) day filtered times series varied over a range of 45 cm/s (18 cm/s) for the along-slope velocity and of 14 cm (10 cm) for the SLA

(Figures 12a and 12b). The 80-110 day filter provided a rather regular signal with an amplitude of 10 cm in the along-slope velocities and 4 cm in the SLA.

Lagged correlations of along-slope velocity anomalies at 100 m for each filter period are shown in Figure 13. The diagrams featured correlations decreasing with distance from Ω' suggesting continuous damping of the propagating signals along the slope (Figures 13a,13b, 13c). The characteristic time of damping (amplitude reduced by half) was about 10 days for the 10-40 day band-passed signals, 20 days for the 30-90 day band-passed signals and about 100 days for the larger period signals. The 10-40 day band-pass filter selected waves with a period of about 20 days and a phase speed of 25± 1 cm/s between km 700 and 1400 (Figure 13a). The 30-90 day band-pass filter provided waves with a period of about 60 days and a phase speed of 20± 2 cm/s between km 600 (49°S) and km 1500 (43°S) (Figure 13b). The 80-110 -day band-pass filter delivered waves with a period of about 100 days and a phase speed of 14± 1 cm/s between km 300 and 1500 km (Figure 13c). The correlation patterns for the three band-passed velocities changed between km 1400 and 1800 (between point C and Ψ', Figure 5a), at a location where the shelf-break abruptly changes orientation (from North to Northeast) and bottom slope steepens (Figures 13a, 13b and 13c). There, phase velocities slightly increased. Beyond km 2000, lagged correlations indicated southwestward propagating patterns. We interpreted those as signals associated with the Brazil-Malvinas Confluence. Between km 1600 and 2000, the lagged composite diagrams suggested interferences between the northward propagating waves and signals from the Confluence.

Composite maps (Figure 14) were built selecting the days with a band-passed velocity amplitude at Ω' larger than the band-pass velocity standard deviation (Figure 12a): 1429, 1461 and 1415 days were considered for the 20-, 60- and 100-day period waves

respectively. The 20-, 60- and 100-day period waves had along-slope wavelengths of about 450, 1000 and 1200 km respectively (Figure 13), and featured an across-slope structure of mode with narrow cores of about 25, 40, and 50 km width respectively (Figures 14 a-e; 14 f-j; 14 k-o). Upstream 49°S, lagged composites suggested two paths, one from the northern Drake Passage and one from the deep argentine basin along the Malvinas Escarpment (Figure 1a). The two contributions combined around 49°S (around km 600 in Figures 13a, 13b and 13c) where the distance between the 1500 m isobath from the Plateau and the 2800 m isobath from the Escarpment reduces to 50 km (Figures 14 a-e; 14f-j; 14 k-o). Two deep passages in the North Scotia Ridge connect the Drake Passage to the Argentine Basin: East of Burwood Bank (EBB) and Shag Rock Passage (SRP) (Figure 1a). The velocity anomaly in the composite maps over the Malvinas Plateau showed patterns suggesting that waves from Drake Passage may proceed through the two passages. This was in agreement with observations showing the SAF crossing the North Scotia Ridge through either EBB or SRP (Artana et al., 2016).

North of 43°S, the signal in the composite maps for the 20- and 60-day waves weakened and stretched along the shelf break while the signals in the composite maps of the 100 day waves became patchy, an indication of interferences with signals coming from the Confluence.

The 60- and 100-day period waves were associated with consistent elongated SLA anomalies of 2 to 3 cm amplitude in the composites (Figures 15b and 15c), which clearly showed the two pathways from the Malvinas Plateau and Escarpment. Signals in the SLA composite for the 20-day period waves were blurry (Figure15a) as these waves had shorter wavelengths, smaller widths, and were more rapidly damped in the model. In contrast, synoptic values of SLA could reach 7 cm for the 20-day period

waves, 5 cm for the 60-day period waves and 2 cm for the 100-day period waves (Figure 12b).

5 Summary and discussion

We used GLORYS12 to examine velocity variations at periods larger than 10 days along the complex Patagonian shelf break (variable direction and steepness). Comparisons with current-meter mooring data from the slope near the complex Brazil-Malvinas Confluence region are stringent tests for model performance. They showed that GLORYS12 lacked energy at periods less than 10 days (Figure 3). All along the slope, GLORYS12 reproduced peaks in SLA energy comparable to those from satellite altimetry, with however more energy at time scales shorter than 20 days.

Statistics over 25 years indicated three types of signals: signals in phase to the south of 47°S at the shelf break, fast propagating signals with phase speed ranging from 140 cm/s to 300 cm/s all along the shelf break, and slower signals in the core of the MC with propagation velocities ranging from 10 cm/s to 30 cm/s.

The large zonal wind stress variations south of 47°S were shown to force in-phase along-slope velocity variations and trigger fast propagating waves at specific locations of the shelf break (Figures 6 and 7). The fast waves (phase speed between 140 and 300 cm/s) departed from distinct sites corresponding to abrupt changes in the shelf break orientation (Figure 6c) . Along-slope velocity anomalies exceeded 15 cm/s at 100 m depth (Figure 7a). The waves impacted the intensity of the inshore jet associated with the SAF-N (Figure 1), which varied from 0 to 30 cm/s at 100 m depth over the 25 years (Figure 10).

The GLORYS12 SLA response to the wind generating the fast waves was large on the continental shelf (SLA composite up to 6 cm) and smaller along the shelf break (composite of 3 cm). Synoptic SLA at the shelf break at 47°S reached peak values larger than 5 cm lasting less than 20 days (Figure 11). Therefore, tracking these waves in present satellite altimetry maps could be challenging.·

Although Brink's model is too idealistic (e.g., Brunner et al., 2019) and requires several assumptions such as a straight coastline with similar slope bathymetry, which are not fulfilled along the Patagonian shelf break, it provided guidance to the interpretation of those waves. Their phase speed and their spatial structure across the slope corresponded to a mode 2 to 4 in Brink's model (Figures 7, 8 and 9). Their positive stage featured increased northward along-slope velocity (5 to 20 cm/s) associated with inshore cross-slope velocities (1 to 2 cm/s). Scaling with Brink's theory predicted positive vertical velocities of the order 5 to 20 m/day associated with inshore horizontal velocities of 1 cm/s in the positive phase (reverse in negative phase). Thus, the fast waves could contribute to enhance transport of nutrients from the MC onto the shelf. Short-term moorings above the 200 m isobath at 41°S and 43.8°S provided evidences of upwelling events lasting 5 to 10 days extending over 500 km at the shelf-break and requiring vertical velocities of the order of 13-29 m/d (Valla and Piola, 2015). The shelf-break fast waves in GLORYS12 had spatial and temporal velocity structures consistent with those of the observed upwelling events described in Valla and Piola (2015).

Three types of propagating waves in the core of the MC were identified. They correspond to periods of about 20, 60 and 100 days, phase speeds of 0.26, 0.19 and 14 cm/s, along-slope wavelengths of 450, 1000 and 1200 km respectively and to a cross-slope mode 2 or 3 with scales ranging from 25 to 50 km. These waves were not

forced by the local winds. Composite velocity anomalies of the order of 6 cm/s (built from 1429, 1461 and 1415 cases for the 20-, 60- and 100-day period waves), associated with these waves were tracked back to the Drake Passage and the Malvinas Escarpment (Figure 14). The forcing mechanisms and the upstream paths of the waves observed in the core of the MC need further investigation.

The waves in the core of the MC changed characteristics at 43°S, accelerated and propagated up to 41°S where they interacted with perturbations coming from the Brazil-Malvinas Confluence. Non linear processes such as scattering, interferences with other signals, damping effects, interaction with the mean flow, refraction and reflection are beyond the scope of this paper. The impact of the trapped waves on the MC transport and location of the Brazil-Malvinas Confluence is under investigation. Extreme transport maxima in the MC at 41°S were related with cyclonic eddies detached from the PF that propagate northward along the 400m isobath (Artana et al., 2018a). The significant energetic peaks in a 30-110 day period band found in the MC transport at 41°S and in the velocity time series associated with the subducted inner branch of the MC at 37°S (Artana et al. 2019) could be associated with trapped waves. Theoretical works also suggested that trapped waves could affect the position of the encounter of the Brazil and Malvinas Current (Lebedev and of Nof, 1996).

Appendix: Trapped waves at 51°S, 47°S and 42°S from Brink and Chapman (1987) linear model

Brink and Chapman (1987) considered a linear, inviscid problem with constant rotation, horizontally uniform stratification (N(z)), and an alongshore non varying bottom topography (h(x)). Brink and Chapman's toolbox computes modal structures from bottom topography h(x), offshore stratification $N^2(z)$, mean flow (V(x,z)), for a given frequency and wavenumber. We applied the toolbox to 3 sections (51°S,47°S and 42°S) shown in Figure A1.a (pink, red and blue). Following GLORYS12 mean flow values of the Malvinas Current, the idealized mean flow, V(x,z) is composed of one or two northward jets depending on the section (Figure A1.b-d). Taking into account the two-jet structure intensified the mode in the vicinity of the jets. Similarly, following GLORYS12, we chose an idealized stratification weak and uniform along the Malvinas Current (Figure A1.f).

The structure of the modes is dependent on the Burger number : $S = (\alpha N/f)^2$ with α the cross-shore slope in m/m, N the mean coastal Brünt-Väisälä frequency and f the Coriolis parameter (Figure A1.e). Small values of S (S<1) correspond to fast propagating barotropic shelf-waves where the rotation dominates over gravity, while a large value (S>1) of S corresponds to slow-propagating baroclinic waves. S along the three cross-slope sections was lower than one suggesting barotropic modes. The three modes featured larger velocity anomalies near the shelf break for the three sections (Figure A2). The mode 3 featured inshore across slope velocity associated with positive vertical velocities for the three sections (Figure A3).

For 1500 km (consistent with the length of the Patagonian slope of the order of 3000 km), the theory provided waves with periods ranging between 1 to 30 days and phase

speeds between 30 and 800 cm/s (Figure A4.a and Figure A4.b). We focused on probably realistic wavelengths ranging between 600 and 1500 km for which theory predicts low dispersive mode 2-4 waves (Figure A4.b) with phase speeds ranging from 50 to 300 cm/s (Figure A4.b).

Acknowledgments:

We thank the Editor, Don Chambers, an anonymous reviewer and Josep Lluís Pelegrí for a number of constructive comments and suggestions. We are grateful to the CNES (Centre National d'Etudes Spatiales) for constant support. This study is a contribution to EUMETSAT/CNES DSP/OT/12-2118. Léa Poli acknowledges support from Sorbonne Université and Camila Artana from a CNES Postdoc Scholarship. The satellite data and model outputs are available at Copernicus Marine Environment Monitoring Service (CMEMS; http://marine.copernicus.eu/) and the in situ data are available at SEANOE (www.seanoe.org ; cf. https://doi.org/10.17882/51479, https://doi.org/10.17882/51483 and https://doi.org/10.17882/51492).

References :

Archer, M. R., Li, Z., & Fu, L.□L. (2020). Increasing the space–time resolution of mapped sea surface height from altimetry. Journal of Geophysical Research: Oceans, 124, e2019JC015878. https://doi.org/10.1029/2019JC015878.

Artana, C., R. Ferrari, Z. Koenig, M. Saraceno, A. R. Piola, and C. Provost (2016). Malvinas Current variability from Argo floats and satellite altimetry, Journal of Geophysical Research, Oceans, 121, 4854– 4872, doi:10.1002/2016JC011889.

Artana, C., Lellouche, J.-M., Park, Y.-H., Garric, G., Koenig, Z., Sennéchael, N., et al. (2018). Fronts of the Malvinas Current System: Surface and subsurface expressions revealed by satellite altimetry, Argo floats, and Mercator operational model outputs. Journal of Geophysical Research. Oceans, 123, 5261– 5285. https://doi.org/10.1029/2018JC013887

Artana C., Provost C., Lellouche J.-M. , Rio M.-H., Ferrari R. & Sennéchael N. (2019). The Malvinas Current at the Confluence With the Brazil Current: Inferences From 25 Years of Mercator Ocean Reanalysis. Journal of Geophysical Research, Oceans, https://doi.org/10.1029/2019JC015289

Ballarotta, M., Ubelmann, C., Pujol, M. I., Taburet, G., Fournier, F., Legeais, J. F., et al. (2019). On the resolutions of ocean altimetry maps. Ocean Science, 15(4), 1091–1109. https://doi.org/10.5194/os-15-1091-2019

Barré, N., Provost, C., Renault, A., & Sennéchael, N. (2011). Fronts, meanders and eddies in Drake Passage during the ANT-XXIII/3 cruise in January–February 2006: A satellite perspective. Deep Sea Research Part II: Topical Studies in Oceanography, 58(25-26), 2533–2554. https:// doi.org/10.1016/j.dsr2.2011.01.003

Brink, K. H. (1982). A comparison of long coastal trapped wave theory with observations off Peru. Journal of Physical Oceanography, 12, 897–913.

Brink, K. H., & Chapman, D. C. (1987). Programs for computing properties of coastal-trapped waves and wind-driven motions over the continental shelf and slope (Tech. Rep. WHOI-87-24, 122 pp). Woods Hole, MA: Woods Hole Institution.

Brink, K. H. (1989). Energy conservation in coastal-trapped wave calculations. Journal of Physical Oceanography, 19, 1011–10*16.*

Brunner K., D. Rivas, K.M.M. Lwiza (2019). Application of classical coastal trapped wave theory to High Scattering regions. Journal of Physical Oceanography, 49, 2201-2216, https://doi.org/10.1175/JPO-D-18-0112.1

Cabanes, C., Grouazelm, A., von Schuckmann, K., Hamon, M., Turpin, V., Coatanoan, C., Guinehut, S., Boone, C., Ferry, N., Boyer Montegut, C., Carval, T., Reverdin, G., Pouliquen, S., & Le Traon, P. Y. (2013). The CORA dataset: Validation and diagnostics of in-situ ocean temperature and salinity measurements. Ocean Science, 9(1), 1– 18. https://doi.org/10.5194/os-9-1-2013

Ferrari R., Artana C., Saraceno M., Piola A.R. & Provost C. (2017). Satellite altimetry and current-meter velocities in the Malvinas Current at 41°S: Comparisons and Modes of variation. Journal of Geophysical Research, Oceans, https://doi.org/10.1002/2017JC013340

Lebedev I. and Nof D., Collision of boundary currents: beyond a steady state, Deep Sea Research Part I, https://doi.org/10.1016/S0967-0637(96)00127-6

Lellouche, J.-M., Greiner, E., Le Galloudec, O., Garric, G., Regnier, C., Drevillon, M., Testut, C.-E., Bourdalle-Badie, R., Gasparin, F., Hernandez, O., Levier, B., Drillet, Y., Remy, E., & Le Traon, P.-Y. (2018). Recent updates on the Copernicus Marine Service global ocean monitoring and forecasting real-time 1/12° high resolution system. Ocean Science, 14, 1093– 1126. https://doi.org/10.5194/os-2018-15

Paniagua G.F., Saraceno M., A.R. Piola, R. Guerrero, C. Provost, R. Ferrari, L.S. lago and C. I. Artana (2018). Malvinas Current at 40-41°S: First assessment of temperature and salinity variability. Journal of Geophysical Research, Oceans, 123, 8, https://doi.org/10.1029/2017JC013666

Piola A.R., Franco B.,C., E.D. Palma & M. Saraceno (2013). Multiple jets in the Malvinas Current. Journal of Geophysical Research, Oceans, https://doi.org/10.1002/jgrc.20170

Pujol, M.-I., Faugère, Y., Taburet, G., Dupuy, S., Pelloquin, C., Ablain, M., & Picot, N. (2016). DUACS DT2014: The new multi-mission altimeter data set reprocessed over 20 years. Ocean Science, 12(5), 1067– 1090. https://doi.org/10.5194/os-12-1067-2016

Romero, S. I., Piola, A. R., Charo, M., and Garcia, C. A. E. (2006). Chlorophyll-a variability off Patagonia based on SeaWiFS data, Journal Geophysical Research, Oceans, 111, C05021, doi:10.1029/2005JC003244.

Smith, W. H. F., and Sandwell, D. T. (1994). Bathymetric prediction from dense satellite altimetry and sparse shipboard bathymetry, *J. Geophys. Res.*, 99(B11), 21803– 21824, doi:10.1029/94JB00988.

Spadone, A., & Provost, C. (2009). Variations in the Malvinas Current volume transport since October 1992. Journal of Geophysical Research, Oceans, *114*, C02002. https://doi.org/10.1029/2008JC004882.

Szekely, T., Gourrion, J., Pouliquen, S., & Reverdin, G. (2016). CORA, Coriolis, Ocean Dataset for Reanalysis. SEANOE. https://doi.org/10.17882/46219

Taburet, G., Sanchez-Roman, A., Ballarotta, M., Pujol, M.-I., Legeais, J.-F., Fournier, F., Faugere, Y., and Dibarboure, G. (2019). DUACS DT2018: 25 years of reprocessed

sea level altimetry products, Ocean Sci., 15, 1207–1224, https://doi.org/10.5194/os-15-1207-2019.

Valla, D., and A. R. Piola (2015). Evidence of upwelling events at the northern Patagonian shelf break, Journal of Geophysical Research, Oceans, 120, 7635– 7656, doi:10.1002/2015JC011002.

Vivier, F., & Provost, C. (1999). Direct velocity measurements in the Malvinas Current, *Journal of Geophysical Research*, Oceans, 104(C9), 21083– 21103, doi:10.1029/1999JC900163.

Vivier, F., C. Provost, & M. Meredith (2001). Remote and local forcing in the Brazil Malvinas Region, Journal of Physical Oceanography, 31, 892–913, doi: 10.1175/1520-0485.

Figure Captions :

Figure 1 :

a) Bathymetry of the Southwest Atlantic (in m) from ETOPO6.2 (update from Smith and Sandwell, 1994). Three passages connecting the Argentine Basin to the Drake Passage are indicated: West of Burwood Bank (WBB), East of Burwood Bank (EBB), and Shag Rocks Passage (SRP). White isolines correspond to 300m and 1500m isobath.

b) mean surface velocities (arrows) and mean surface velocities intensity in cm/s (color) from GLORYS12 over the period 1993-2017.

c) mean surface EKE from GLORYS12 over the period 1993-2017 in $(cm/s)^2$

d) mean values of surface chlorophyll-a concentration (in mg/m^3) derived from MODIS satellite data. Note the long continuous high values (>2.5 mg/m^3) at the shelf break. (2002-2017).

The mean locations of the northern branch of the SAF (SAF-N) is represented with a black dashed line, that of the main SAF (SAF) with a continuous black line (defined as in Barré et al., 2011), that of the Brazil Current front (BCF) with a cyan line (defined as in Ferrari et al., 2017). The white segment at 41°S in a) marks the sites of successive mooring deployments.

Figure 2 :

Sea level anomaly variance preserving spectra as a function of latitude (SLA was averaged in a longitude band between the 300 and 1700 m isobaths) a) from satellite altimetry DUACS product b) from Mercator reanalysis GLORYS12. White lines at 41°S correspond to the location of the moorings.

The gap between 50.5°S and 48°S corresponds to a region with zonal isobaths (Figure 1a). Color bar in cm^2. c) Sea level anomaly variance preserving spectra averaged between 48°S and 43°S for GLORYS12 (red) and for satellite altimetry DUACS product (black). Dashed lines correspond to a 90% confidence limit.

Figure 3 :

Mean Flow and variance ellipses for each current meter at 41°S from 1993-1995 in black, 2001-2003 in blue, 2014-2015 in green and from GLORYS12 in red; all- time series have been smoothed with a 5-day low-pass filter. 0M1 and 1A1 are both from the same location (red dashed line). They are displaced on the figure for sake of lisibility. Black line is the bathymetry from ETOPO6.2 and red line is the model bathymetry.

Figure 4 :

Lagged correlation diagrams of 110-day high-pass filtered along-slope velocities at 100 m depth above the 300 m isobath.

a) points along the slope used for the correlations with locations Φ (53.5°S), Ω (47°S) and Ψ (41°S). Red line is the 300 m isobath. Background is bathymetry (in m). b) along-slope velocity correlations with Φ. X-axis is along-isobath distance from 53.5°S, y-axis is lag in days. Pink dots indicate locations where maximum correlations were obtained at lag 0 day.

c) along-slope velocity correlations with Ω (axes as in b)

d) along-slope velocity correlations with Ψ (axes as in b)

Only significant correlations (above 90% confidence limit) are colored.

Dashed lines correspond to a linear fit of maximum correlations. The slopes provide estimates of the phase velocities b) 250 ± 50 cm/s and 167± 15 cm/s c) 156 ± 15 cm/s for both dashed segments, d) 35 ± 3 cm/s and 210 ± 50 cm/s.

Figure 5 :

a) points along the slope used for the correlations with location Φ' (58.6°W, 53.35°S), Ω' (59.2°W, 47°S) and Ψ' (56°W, 41°S), blue line is the 1500 isobath. Background is bathymetry (in m).

b-d) Lagged correlation diagrams of 110-day high-pass filtered along-slope velocities at 100m depth over isobath 1500 m (in the core of the MC) considering point Φ '(b), Ω' (c), Ψ' (d). X-axis is distance along the isobath and Y-axis is lag in days.

Phase velocities estimated as in Figure 4: c) 23± 2 cm/s d) 30± 2 cm/s

Figure 6:

a. Mean wind stress (1993-2017) from ERA-interim, arrows represent direction and background is intensity (all in Pa)

b. Standard deviation of the zonal wind stress.

c. Lagged correlations between the zonal wind stress at Φ (53°S) and ocean along-slope velocities at 100 m above 300 m isobath over the 25 years of GLORYS12 reanalysis. Only significant correlations are shown. Lagged correlations above the 1500 m isobath are not significant (not shown). X axis is distance from Φ along the isobath, y-axis is lag in days and vertical lines correspond to location of points A,B,C,D, Φ, Ω and Ψ shown in Figure 6a) and b).

Pink dots indicate locations where correlations with the wind were maximum at lag 1 day. Phase velocity were estimated as in figure 4 : between 108 cm/s and 241 cm/s

Stick plot represents the bathymetry gradient along the slope at each colored dot shown in a). Black Arrow represents the north .

Figure 7:

a: Time series of along-slope 110-day high-pass filtered velocity at 100 m above the 300 m isobath at Ω for 2 years (2016-2017 as an example for sake of clarity).Units are in cm/s and shaded area corresponds to the standard deviation.

b, c, and d: along-slope velocity composites at 100 m. They were built considering the dates with velocities exceeding the standard deviation at Φ, Ω and Ψ, respectively (positive phase). The arrows on b) and e) indicate the corresponding wind stress anomaly composite.

e,f and g : Same as b-c-d for the negative phase.

Figure 8 :

a) Location of the three sections examined in the appendix using Brink and Chapman's model. GLORYS12 velocity composites (in cm/s) were produced along the sections (b to g) for comparison with theory. They were built averaging fields at dates when filtered velocities at 100 m over the 300 m isobath exceeded the standard deviation.

b-c) Composite of filtered along-slope velocity along the blue section for positive b) and negative c) phase for the dates when the filtered velocity at 100 m over the 300 m isobath exceeds the standard deviation.

d-e) Composite of along-slope filtered velocity along the red section for positive d) and negative e) phase for the dates when the filtered velocity at 100 m over the 300 m isobath exceeds the standard deviation.

f-g) Composite of along-slope filtered velocity along the magenta section for positive f) and negative g) phase for the dates when the filtered velocity at 100 m over the 300 m isobath exceeds the standard deviation.

Figure 9 :

Frequency-Wavenumber spectrum of along-slope velocities at 100 m depth above the 300 m isobath. Colorbar units: velocity psd. Lines correspond to the dispersion relation for theoretical SBTW modes at 51, 47 and 42°S (Figure A4 in appendix).(black dashed lines : mode 1,black lines : mode 2, grey lines : mode 3, blue lines : mode 4)

Figure 10 :

a) Along slope velocities corresponding to the positive phase of the fast waves at 47°S (Mean flow plus twice the composite of along slope velocity anomalies from Figure 7b)s.THe 47°S vertical section is shown b.

b) Along-slope velocity at 47°S section corresponding to a).

c) Same a) for the negative phase.

d) Along slope velocity at 47°S section corresponding to c).

Colorbar in cm/s.

Figure 11:

a) Time series of GLORYS12 SLA above the 300 m isobath at Ω (47°S).

b-g) Composite of model sea level anomalies (SLA) at the dates of the velocity composites shown in Figure 7. Units are in cm. Only significant values are shown.

b-c-d) SLA for the positive phase at Φ (53.5°S), Ω (47°S), and Ψ (41°S).

e-f-g) SLA for the negative phase.

The arrows on a) and b) indicate the corresponding composite of the wind stress anomaly.

Figure 12: GLORYS12 Along slope velocity anomalies (a) and SLA (b) time series (in black) for year 2013 above the 1500 m isobath at Ω (47°S) and filtered time series with different band-pass filters: 10-40 day (green), 30-90 day (red) and 80-110 day (blue). The three filtered time series are tentatively summed (grey curve).

Figure 13 :

a. Lagged correlations of 10-40 day band-pass filtered along-slope velocities with the velocities at Ω (47°S), y axis is lag in days, x axis is distance along the slope above 1500 m isobath

b. Lagged correlations of 30-90 day band-pass filtered along-slope velocities with the velocities at Ω (47°S), y axis is lag in days, x axis is distance along the slope

c. Lagged correlations of 80-110 day band pass filtered along-slope velocities with the velocities at Ω (47°S), y axis is lag in days, x axis is distance along the slope

Phase velocities estimated as in Figure 4:a) 25± 1 cm/s b) 20± 1 cm/s c) 14± 1 cm/s

Figure 14:

a-e) Lagged composites of 10-40 day band-pass filtered along-slope velocities at 100 m from the dates when the filtered velocity exceeds the standard deviation at Ω (47°S).

f-j) Lagged composites of 30-90 day band-pass filtered along-slope velocities at 100 m from the dates when the filtered velocity exceeds the standard deviation at Ω (47°S).

k-o) Lagged composites of 80-110 day band-pass filtered along-slope velocities at 100 m from the dates when the filtered velocity exceeds the standard deviation at Ω (47°S).

Figure 15:

a) Lag 0 composites of 10-40 day band pass filtered sea level anomalies from GLORYS12 corresponding to selected dates used in Figure 13c.

b) Lag 0 composites of 30-90 day band pass filtered sea level anomalies corresponding to selected dates used in Figure 13h.

c) Lag 0 composites of 80-110 day band pass filtered sea level anomalies corresponding to selected dates used in Figure 13m.

ANNEXE : Theoretical modes

Figure A1: Set up conditions for Brink and Chapman's model application:

a) Bathymetry with the 3 sections under consideration.

b-d) Idealized mean along-slope velocities for the 3 sections (51°S, 47°S, 42°S)

x-axis is the distance in km

e) Mean Burger number as a function of the distance along each section

x-axis is the distance in km and y-axis is the Burger number

f) Mean Brunt Vaisala frequency at km 300 for each section

x-axis is the Brunt vaisala frequency in S-1, y-axis is depth in meters

Figure A2:

First 4 gravest modes of along-isobath velocity computed from Brink & Chapman (1987) toolbox at 51°S, 47°S and 42°S (pink, red and blue sections in Figure A1) (The velocities are normalized by an arbitrary factor - their units are consistent) X axis is across-slope distance; Y axis is depth.

Figure A3 :

Across-isobath and vertical velocity components associated with mode and 4 along section 51°S, 47°S and 42°S (shown in figure A1). Scaling as in Figure A2

Zoom on the upper 1000 m. Positive across-slope velocity corresponds to velocity from the shelf to the open ocean and positive vertical velocity corresponds to upwards velocity.

Figure A4 :

a. Dispersion curves for the first four gravest modes of the 51°S section (pink), 47°S section (red), and for 42°S section (blue). X axis is wavelength in km, y-axis is period in days. Thick lines correspond to mode 1, thick lines with dots to mode 2, thick dashed lines to mode 3 and dashed lines to mode 4.

b. Phase velocity computed for each mode (same color code as a). X-axis is wavelength in km and y-axis in velocity in m/s.

Figure A5:

Surface pressure (SP) for modes 1 to 4 along sections at 51°S, 47°S and 42°S.Units in dyn/cm^2 (1 dyn/cm^2 = 0.1Pa).

FIGURES:

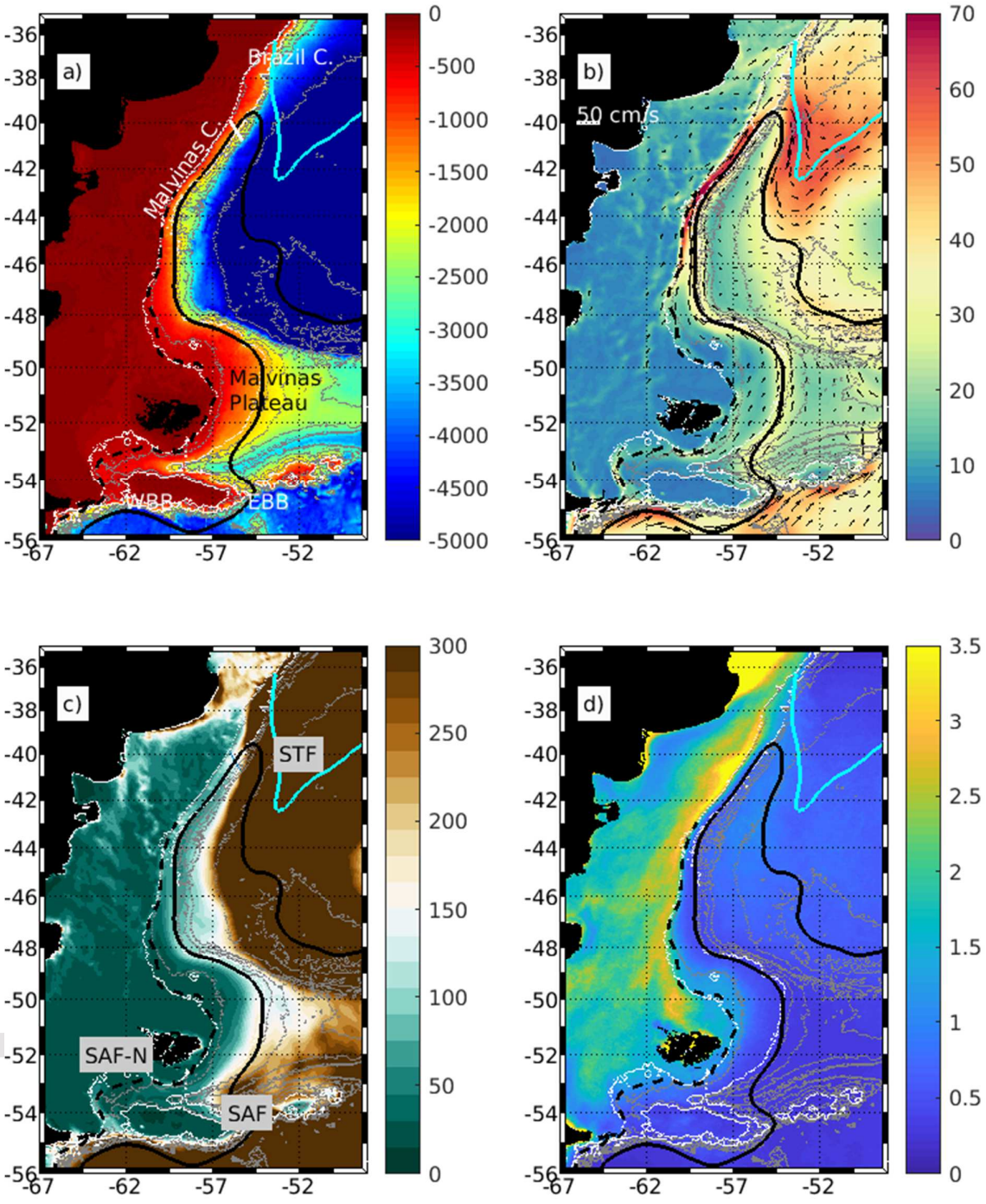

Figure 1

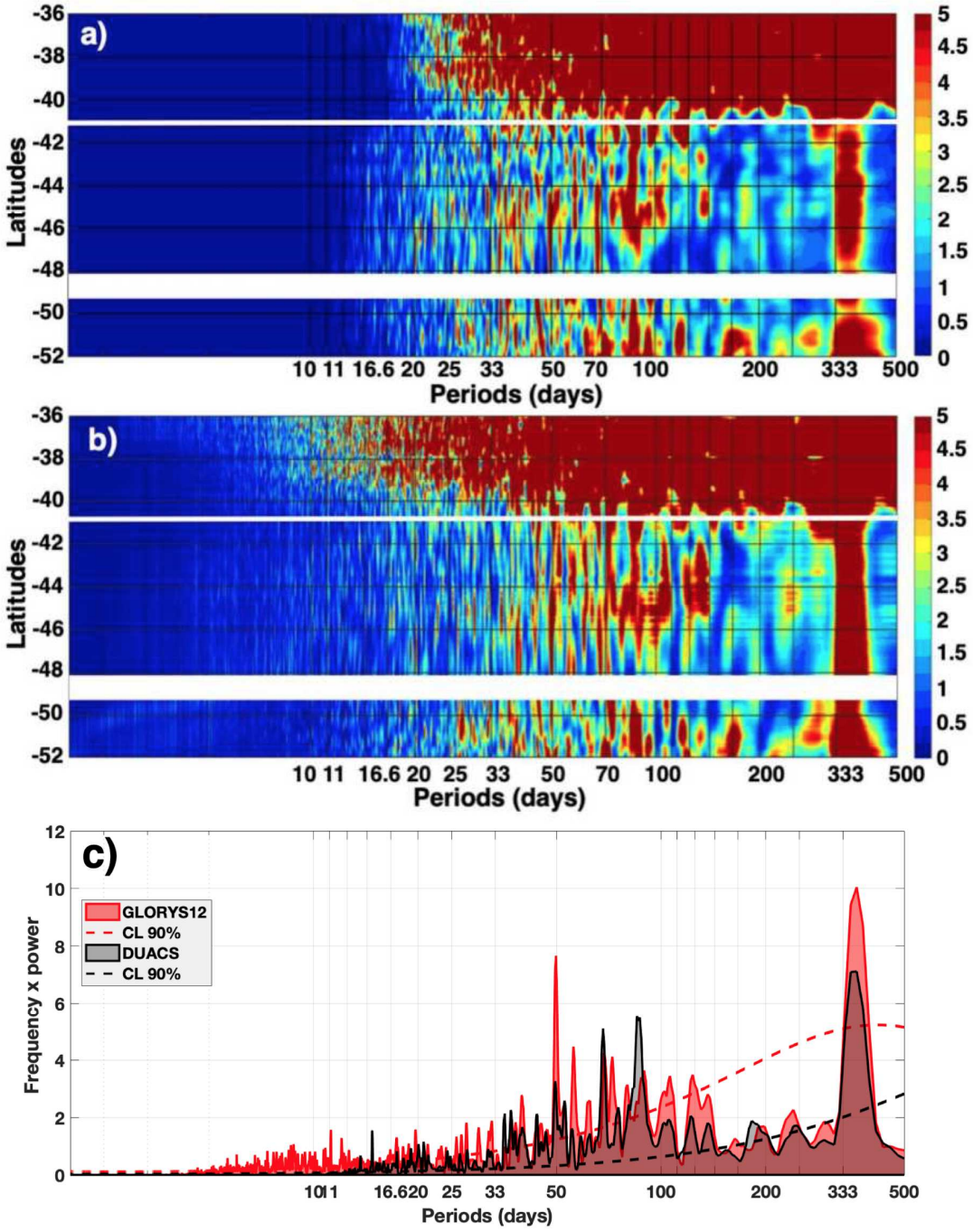

Figure 2

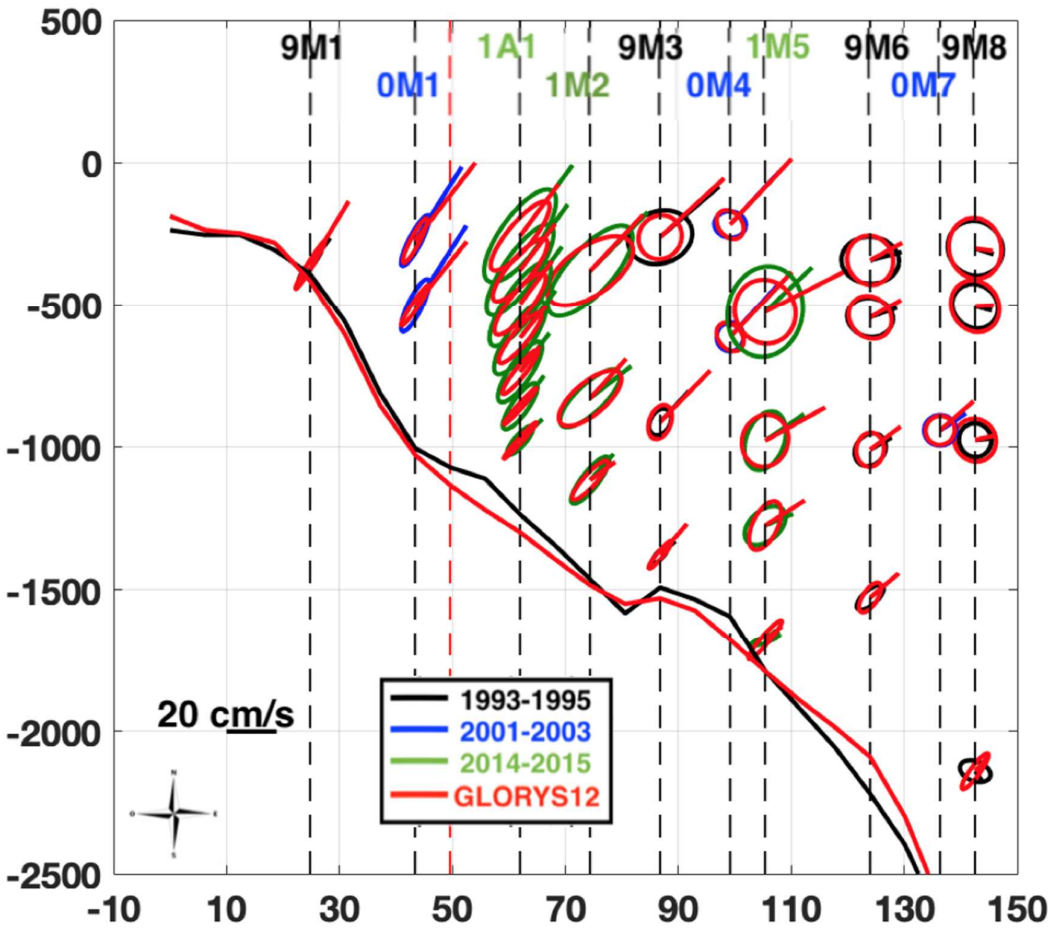

Figure 3

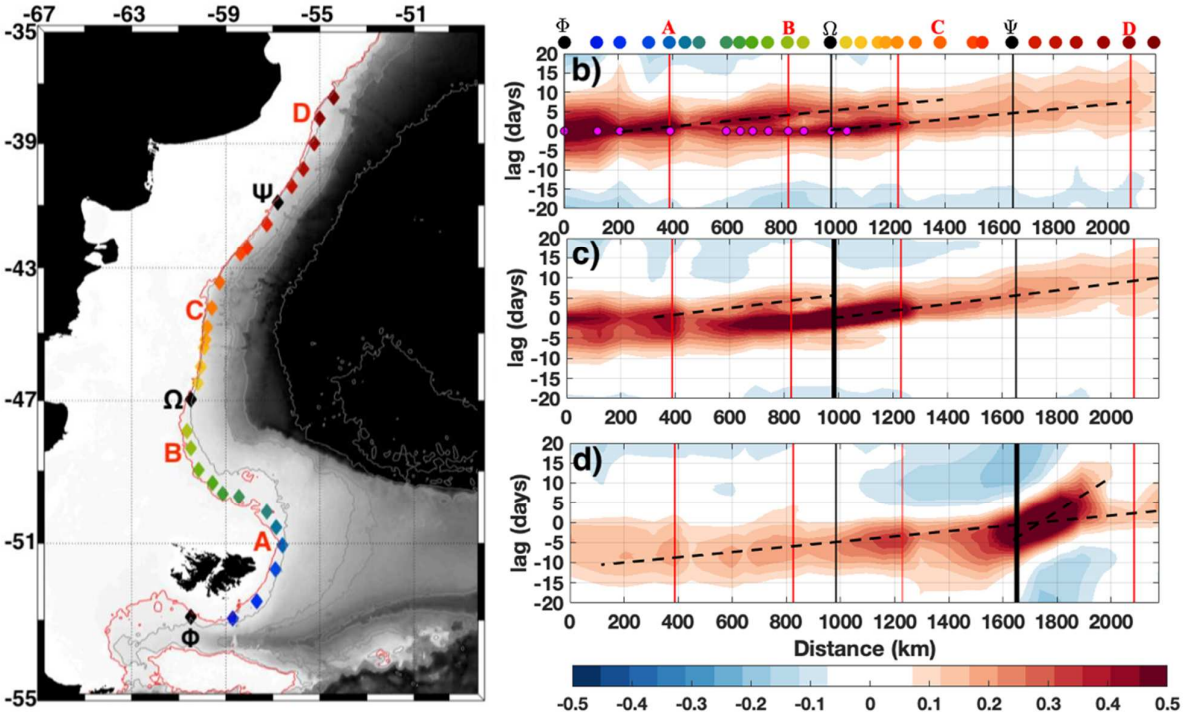

Figure 4

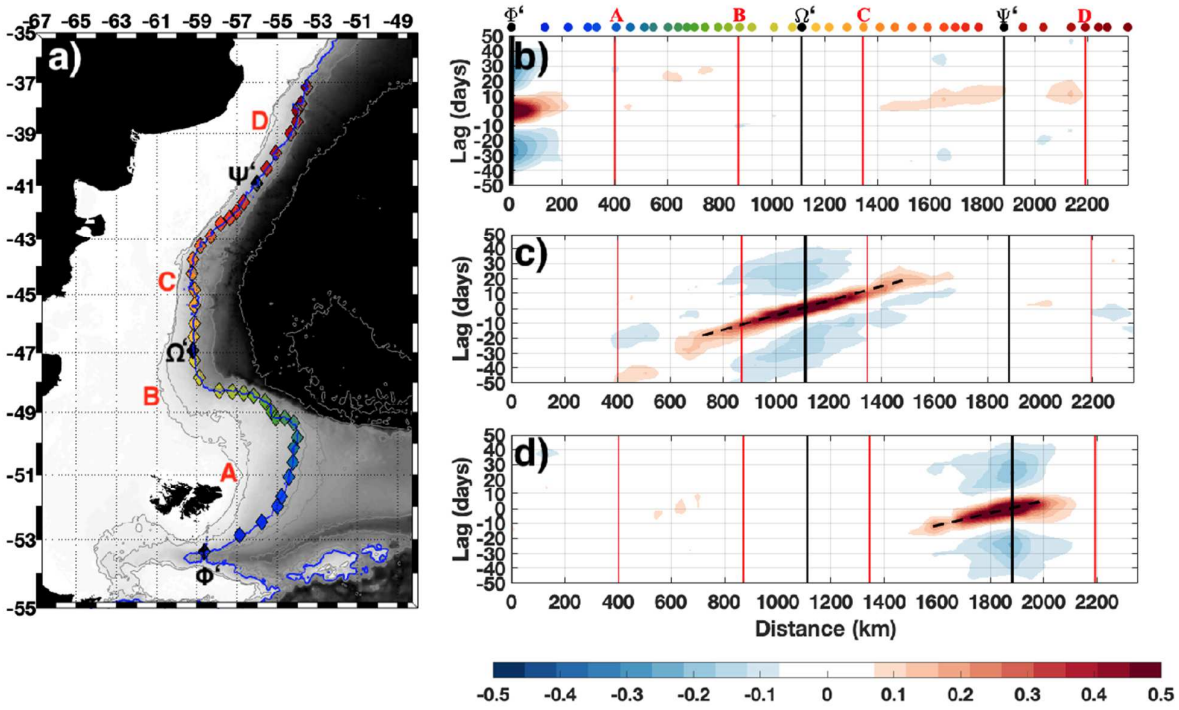

Figure 5

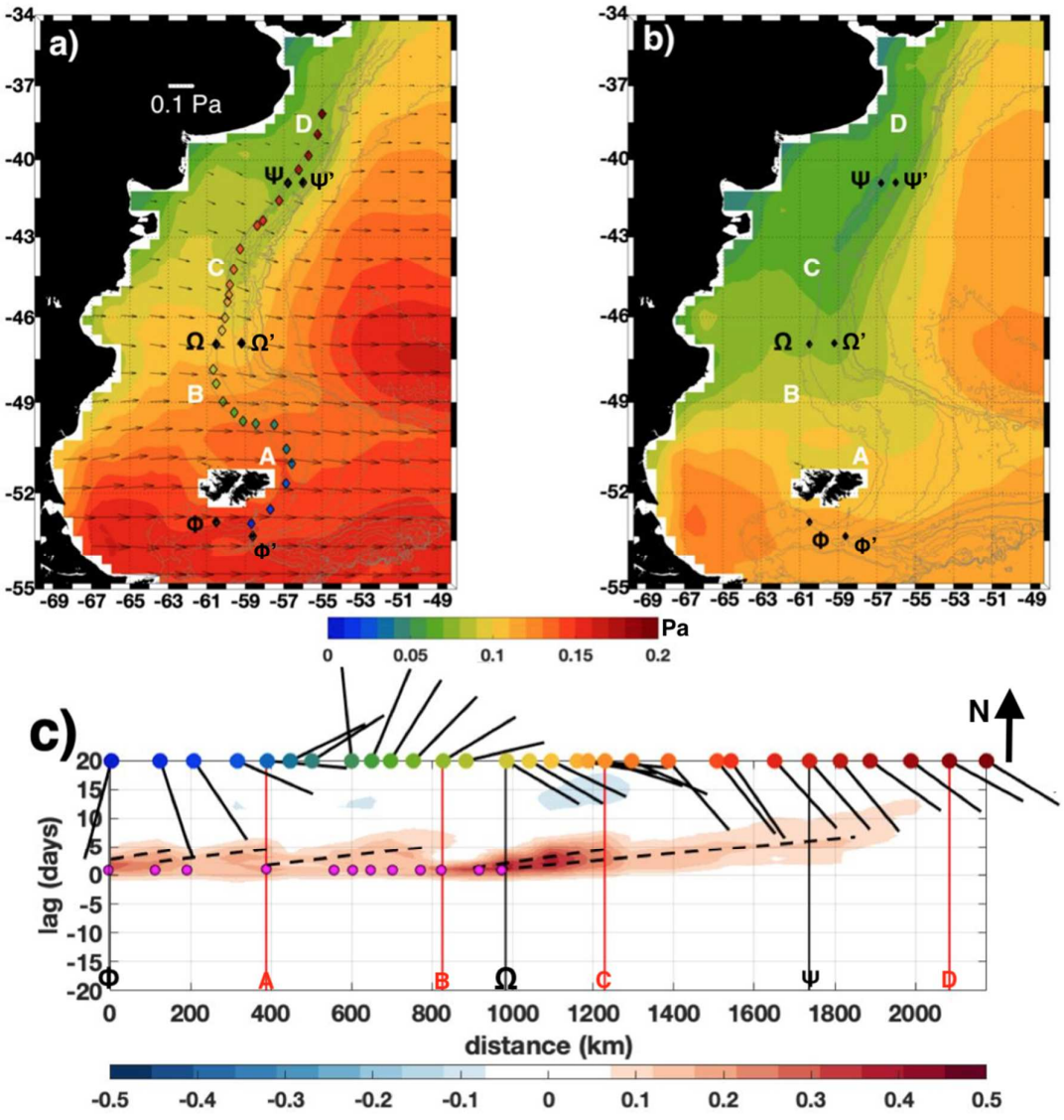

Figure 6

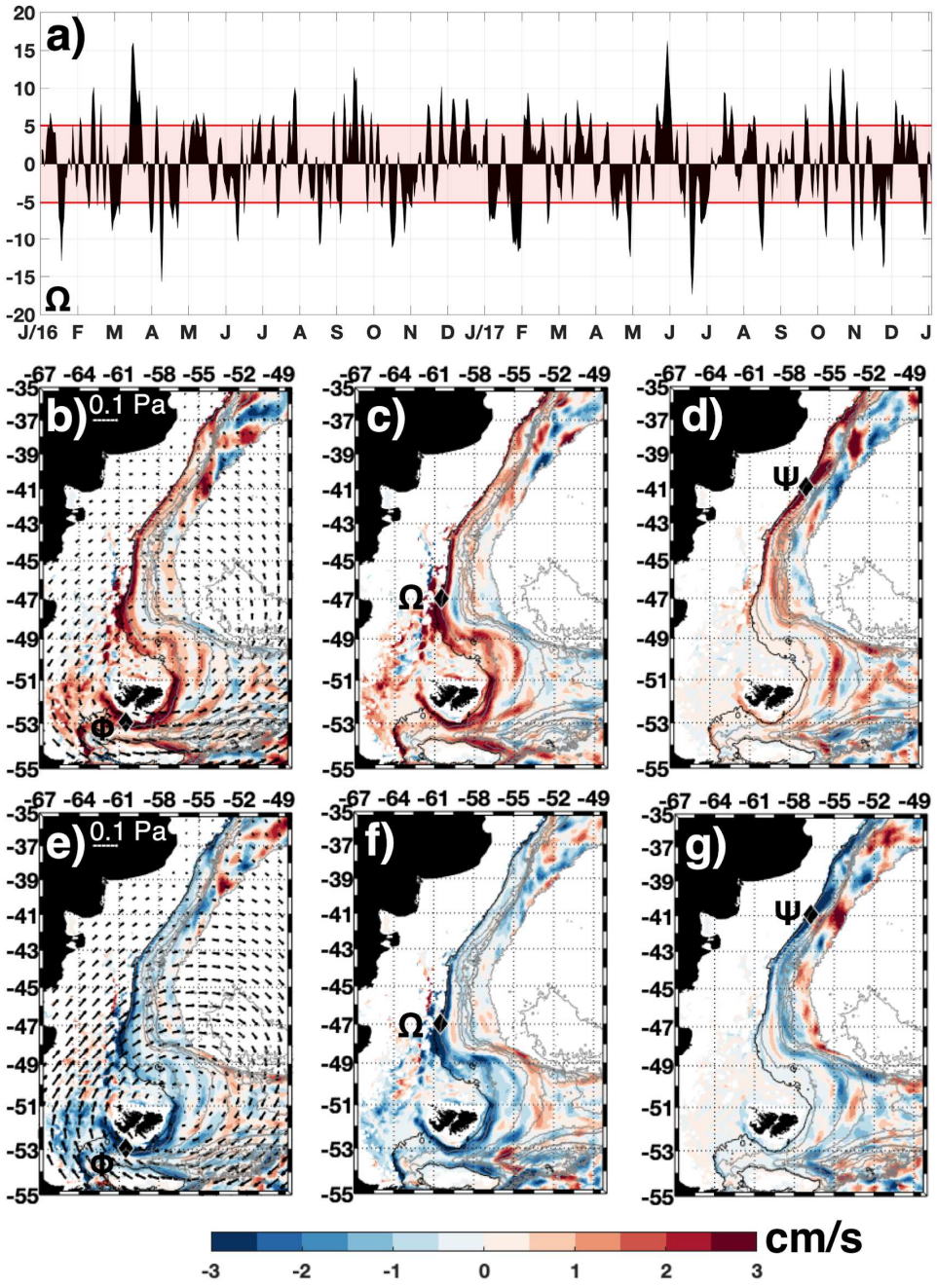

Figure 7

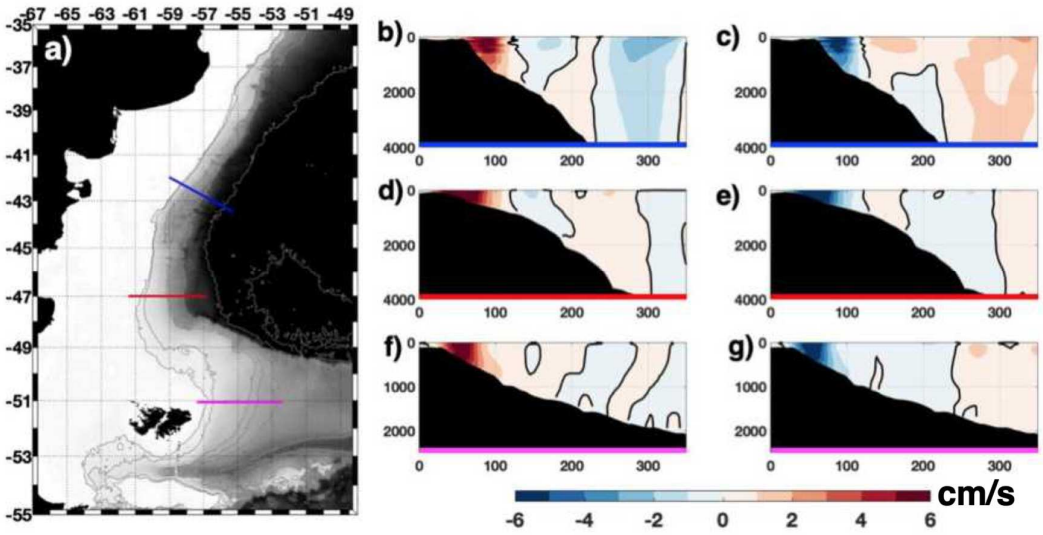

Figure 8

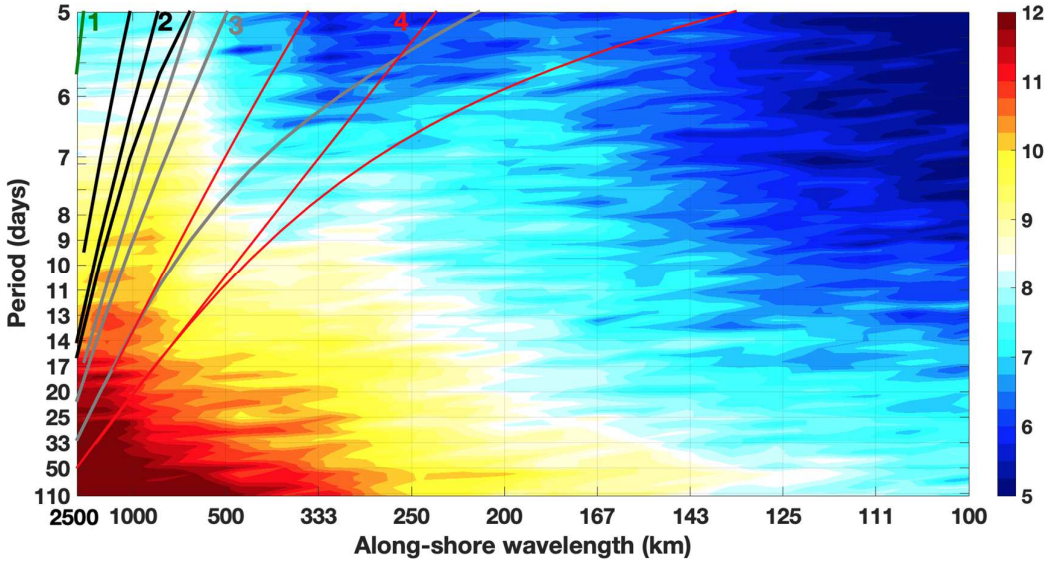

Figure 9

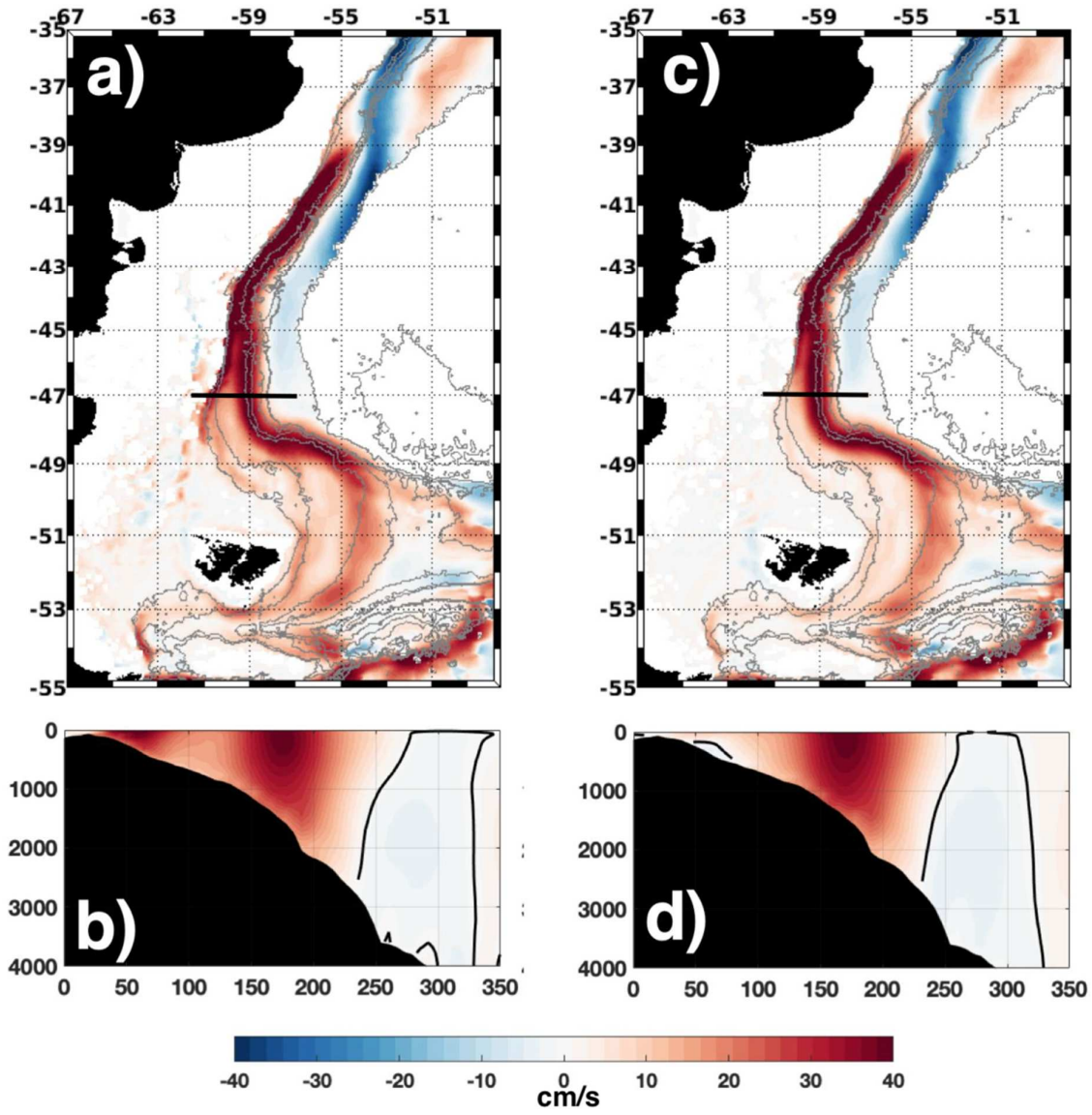

Figure 10

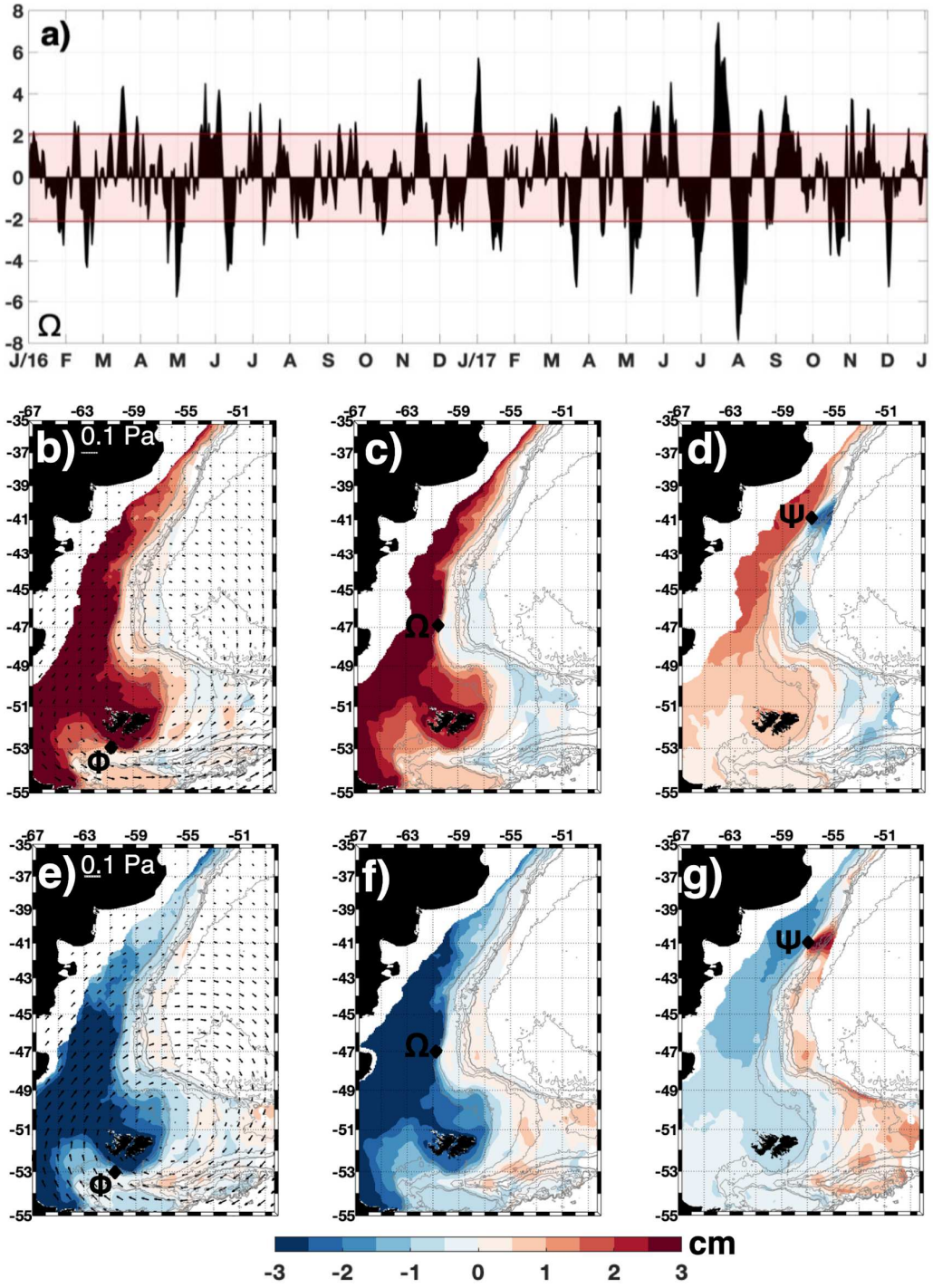

Figure 11

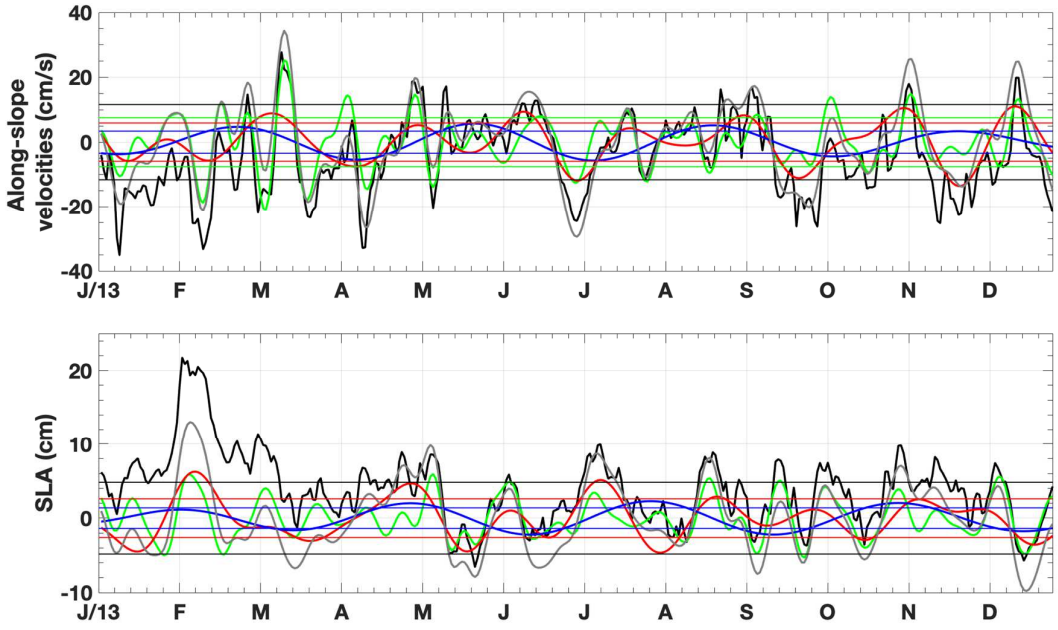

Figure 12

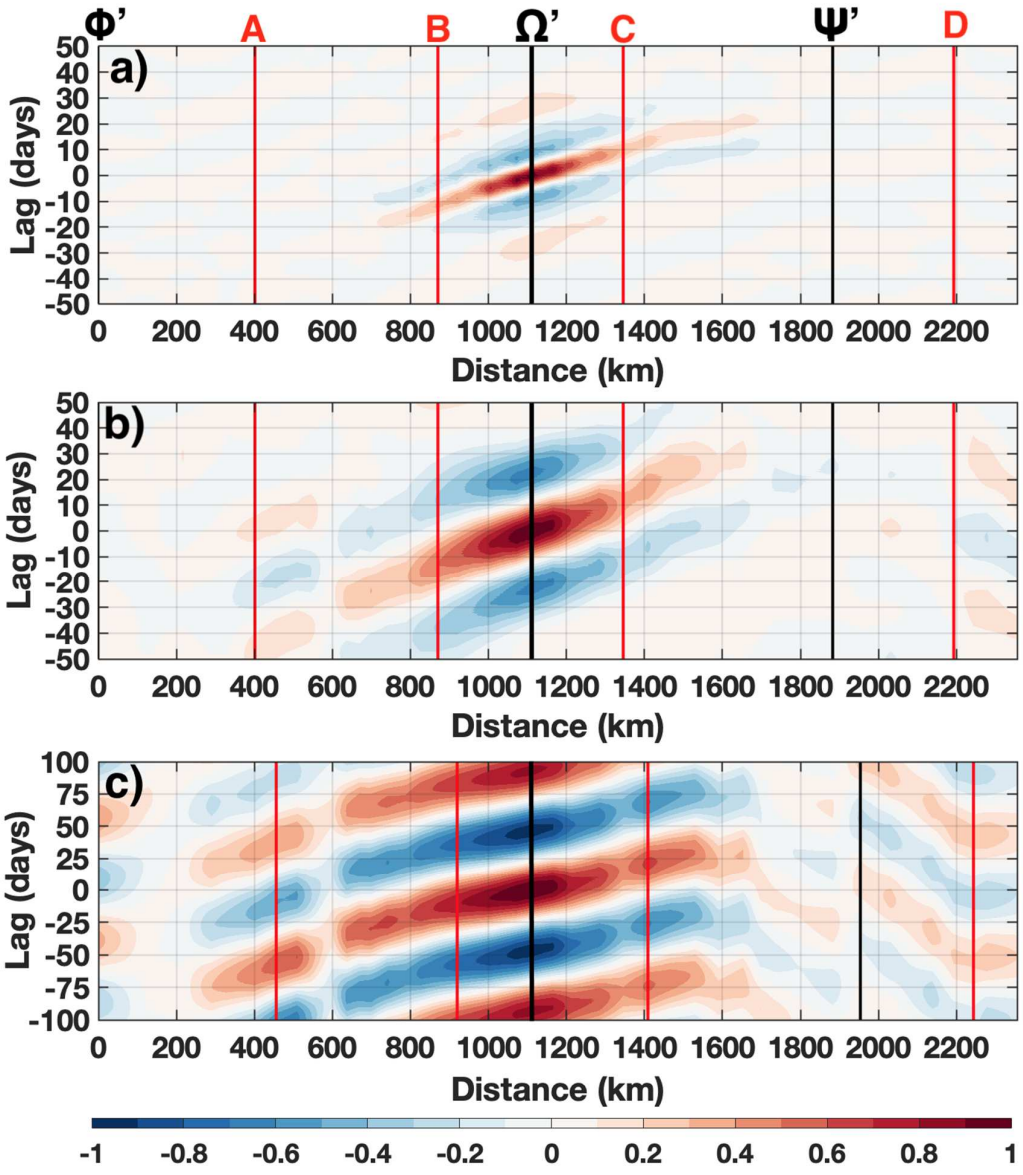

Figure 13

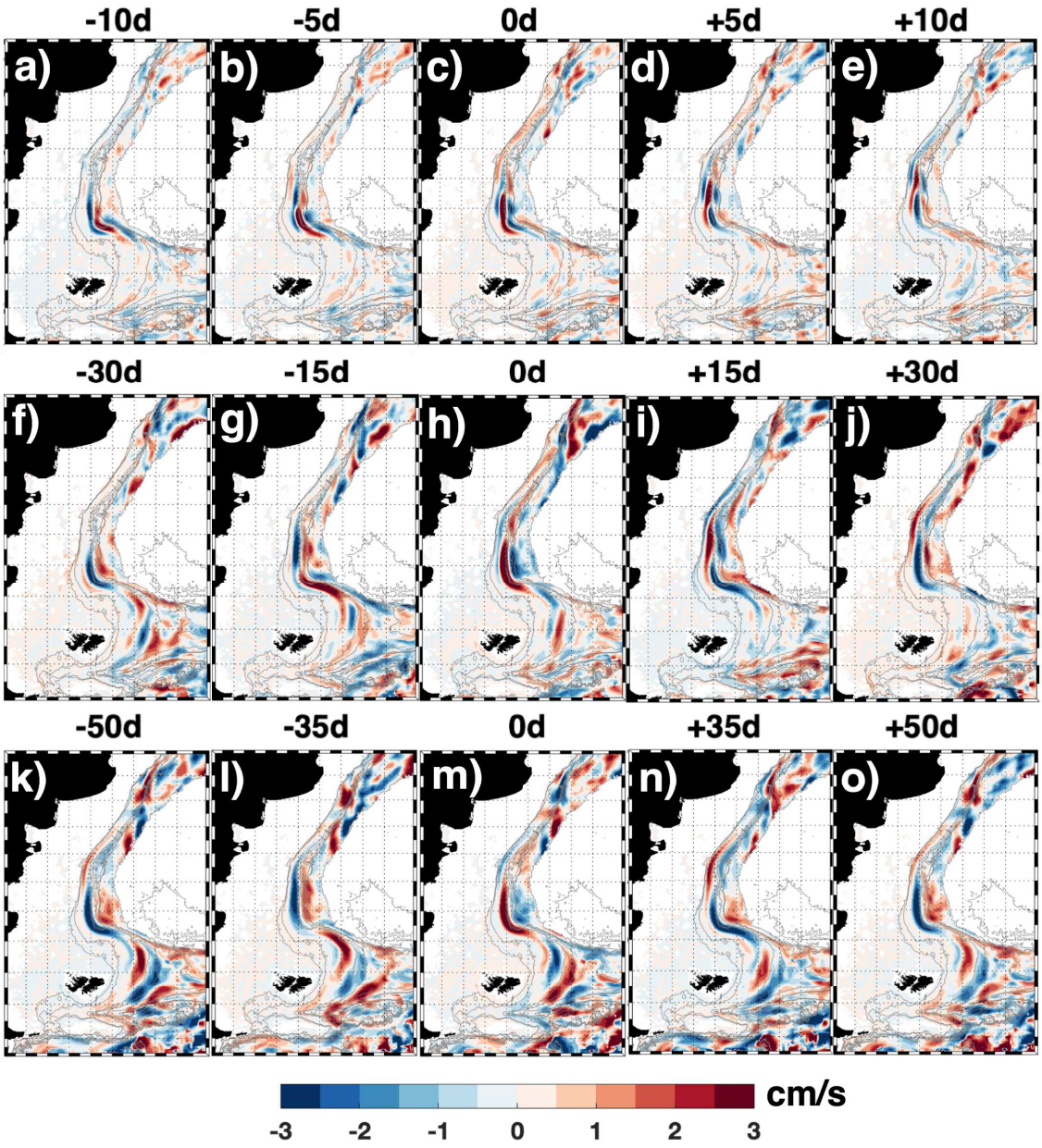

Figure 14

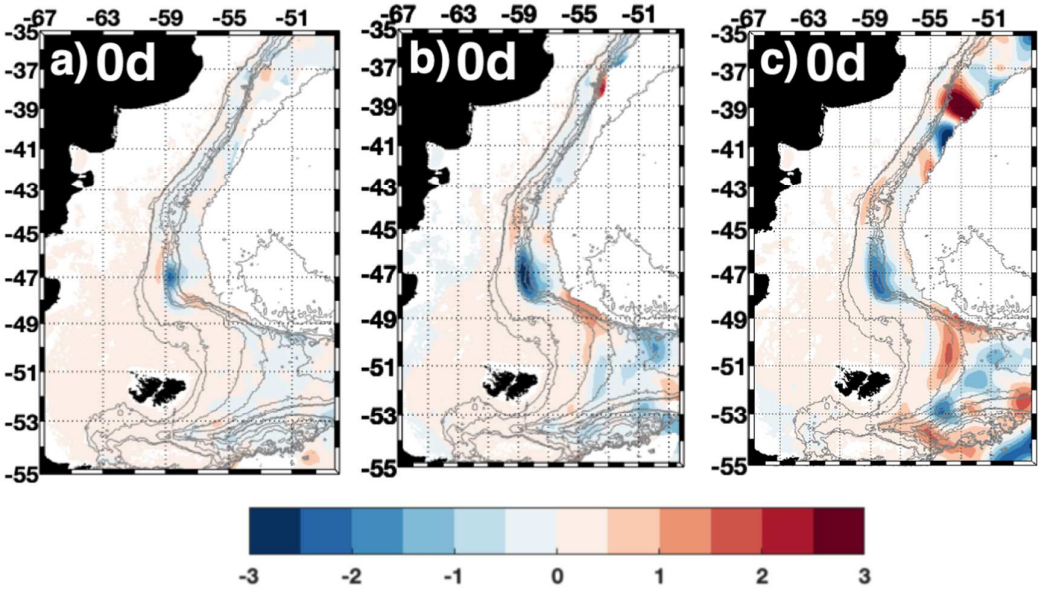

Figure 15

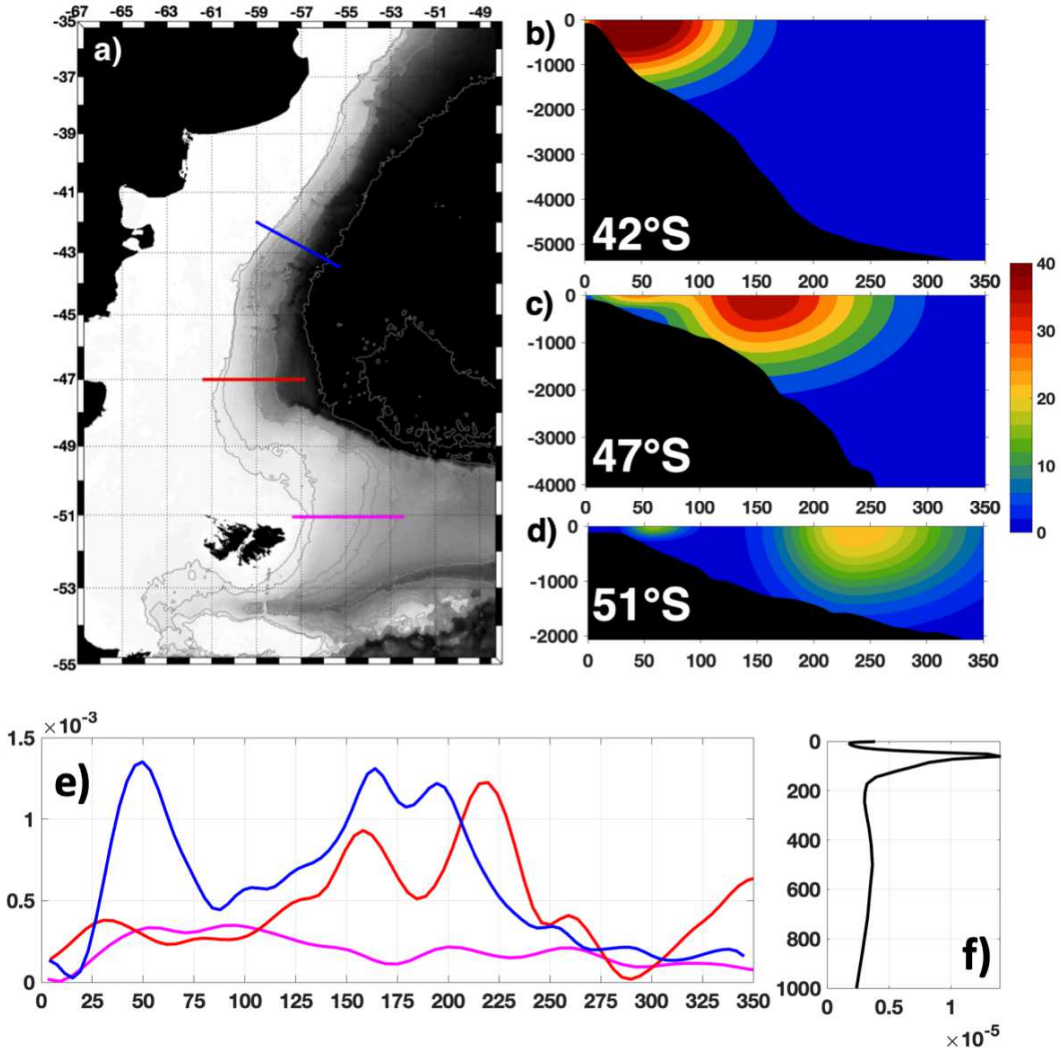

Figure A1

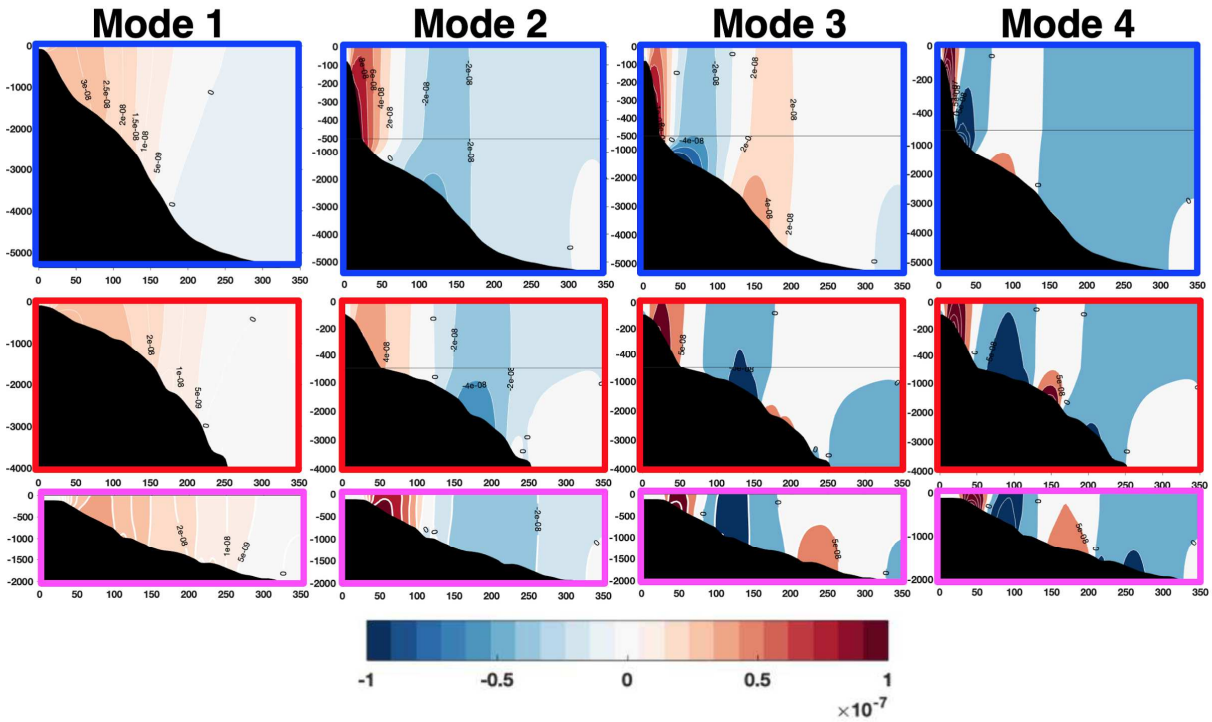

Figure A2

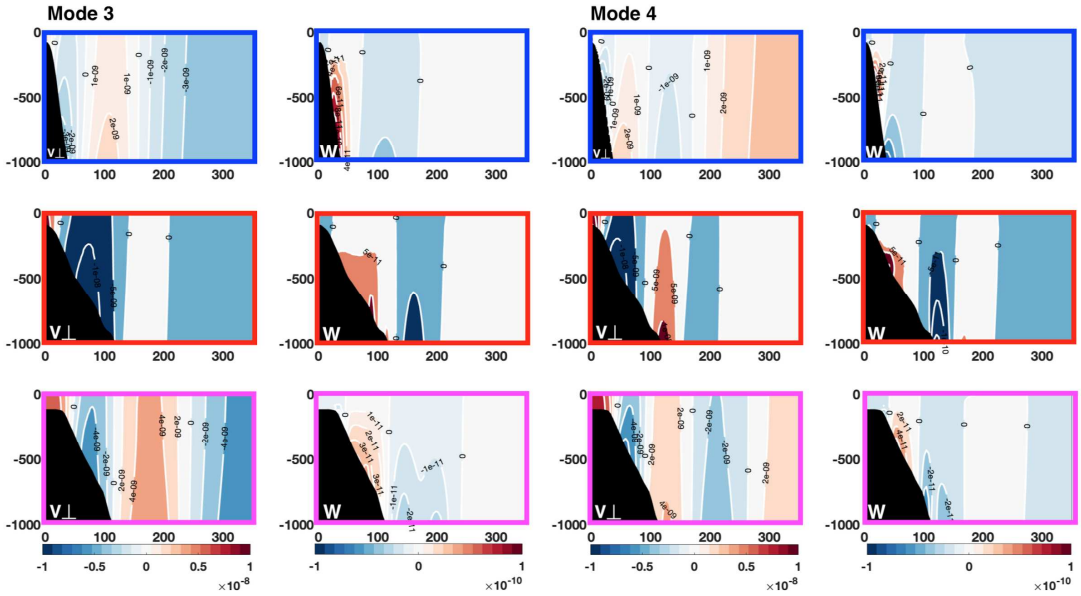

Figure A3

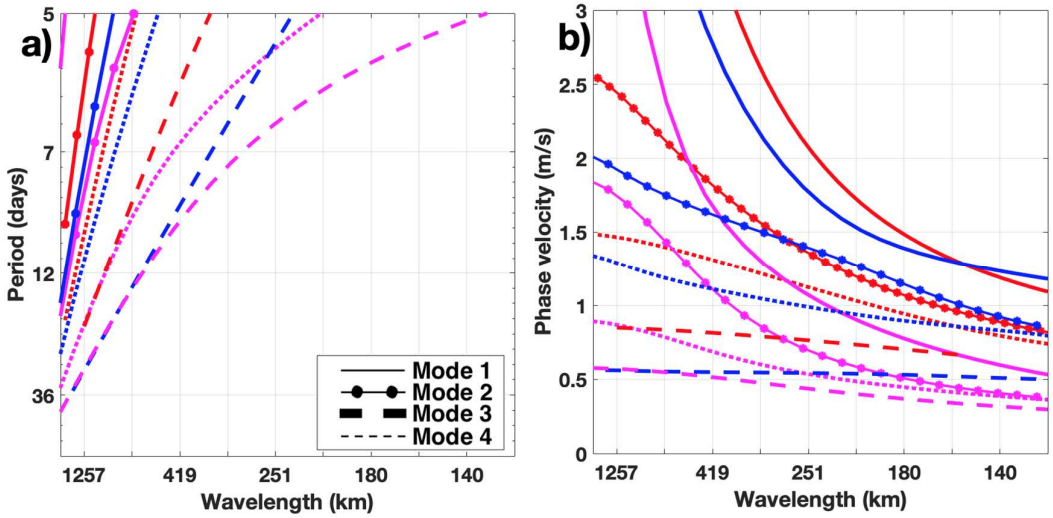

Figure A4

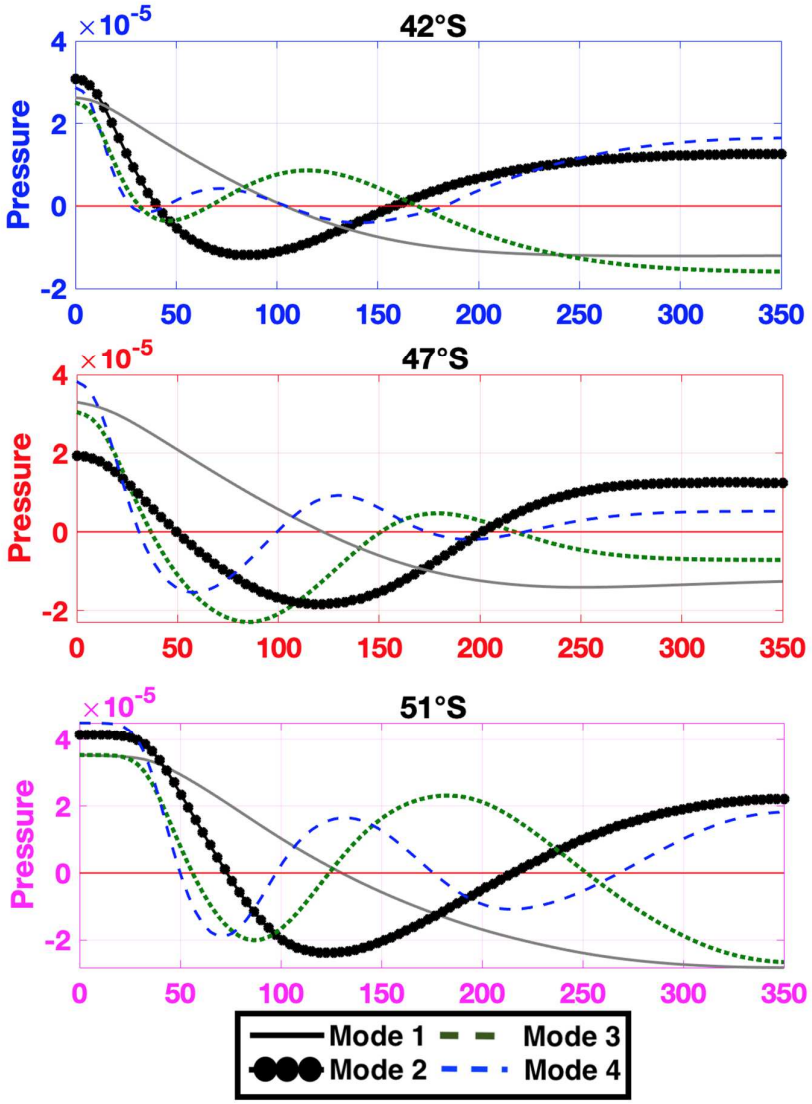

Figure A5